THE STUDY OF DNA DYNAMICS ON GLASSY CARBON ELECTRODE SURFACES

by

D. M. H. KAUSHALYA PERERA

B.S., The Open University of Sri Lanka, 2009

A THESIS

Submitted in partial fulfillment of the requirements for the degree

MASTER OF SCIENCE

Department of Chemistry
College of Arts and Sciences

KANSAS STATE UNIVERSITY
Manhattan, Kansas

2014

Approved by:

Major Professor
Daniel. A. Higgins

Copyright

Abstract

The potential-dependent reorientation dynamics of double stranded DNA (ds-DNA) covalently attached to planar glassy carbon electrode (GCE) surfaces were studied in this thesis. The orientation of ds-DNA was investigated via the distance-dependent quenching of fluorescence from a 6–carboxyfluorescein (FAM6) flurophore to the electrode surface. The fluorophore was covalently bound to the distal end of the DNA. Fluorescence microscopy was employed for optical detection of FAM6 fluorescence and hence the DNA dynamics. The variation of the fluorescence from the dye with electrode potential is attributed to distance-dependent dipole-electrode energy transfer. Application of positive potentials (i.e., +0.2 V vs. open circuit potential, OCP) to the GCE caused the ds-DNA to align approximately parallel to the surface, yielding strong FAM6-electrode energy transfer and low fluorescence intensity. With the switching of the potential towards negative values (i.e., -0.4 V vs. OCP) the ds-DNA realigned perpendicular to the GCE surface leading to a reduction in energy transfer and high fluorescence intensity.

Initial DNA reorientation upon a change in electrode potential is very fast. These fast dynamics have been observed and characterized in a number of previous publications. We have observed subsequent slow dynamics that we attribute to slow orientational relaxation of the DNA. Our observations were first reported by Q. Li, et al., J. Am. Chem. Soc. 2012, 134, 14467. In this thesis, this prior work is extended to verify the reproducibility of these new dynamics and to eliminate the possibility of certain artifacts as their source. Specifically, the experiments are repeated using a new cell design and a different buffer. In the primary experiments performed in this thesis, the dependence of the DNA reorientation dynamics on surface coverage was investigated by observing the fluorescence modulation as a function of probe concentration in the functionalization bath. Concentrations of 0.25, 1.0 and 1.5 μM 35-mer ds-DNA were employed. Electrodes functionalized at these concentrations have ds-DNA surface coverages of 1.18×10^{12}, 3.24×10^{12} and 4.26×10^{12} cm^{-2}, respectively. With increasing concentration of the DNA probe, the reorientation time constant at positive applied bias (vs. OCP) increased, indicting reorientation was slowed. In contrast, the time constant decreased with the negative applied bias (vs. OCP) indicating faster orientational relaxation. The possible origins for the observed trends in the reorientation time constant are discussed.

Table of Contents

List of Figures

List of Tables

Acknowledgements

I would like to offer my appreciation to my advisor Dr. Higgins for his immense guidance and support throughout my Master's work. Without his guidance, I would not have been able to complete this work. It was a wonderful experience to work under him.

I would also like to thank Dr. Jun Li for giving me advice on my research which was very valuable indeed. I would like to thank Dr.Yifen Li and Dr. Lateef Sayeed for helping out with my work initially, all my group members, past and present group members of Ito group, Luxi Swisher, Steven Klankowski and Zi Li for their help in this project. I appreciate the knowledge and advice they shared with me.

I also like to thank my committee member Dr. Christine Aikens and everyone at Kansas State University Chemistry department for this wonderful opportunity and specially Mr. James Hodgson and Mr. Ron Jackson for helping me in preparing devices. Their help is greatly appreciated.

I would like to thank my family members, specially my mother for being my inspiration, my sister and brother-in-law for all their support and guidance as well as helping me out in my thesis work and all my friends for their encouragement and support without which I would not have been able to achieve this goal.

Dedication

I dedicate this work to my loving family.

Chapter 1 Introduction

1.1 Background

Investigations of the field-induced dynamics of DNA bound to electrode surfaces have gained a significant amount of attention in recent years, mainly due to their applications in DNA related research. This interest is largely driven by the desire to develop DNA based sensors and microarrays. Though a vast number of optical methods such as fluorescence detection, surface Raman scattering spectroscopy, surface plasmon resonance (SPR), chemiluminescent detection and colorimetric detection have been used for DNA sensing,[1] electrochemical methods have proven to be of much importance because they can be performed in a label-free manner. It has been observed that DNA layers respond to applied electric fields and those electric fields can be used to manipulate and enhance the binding efficiency of complementary DNA strands. Detection in label free electrochemical method is based on the modifications of properties such as capacitance or an electrochemical response due to DNA. A perfect match between the probe DNA and its complementary target will produce the most stable double stranded DNA (ds-DNA). Mismatches even down to a single base decrease ds-DNA stability and will cause a signal modification. Although these methods have already been demonstrated, a deeper understanding is required in order for these methods to be used in successive commercial devices.

1.1.1 DNA hybridization sensors

DNA biosensors, which are also known as gene sensors, are promising tools with applications in areas such as forensic science, DNA diagnostics, biological research, pathology, food safety and gene analysis.[2,3,5] DNA detection is based on the sequence-specific hybridization between a probe and its complementary target DNA.[4,5] These sensors can be categorized according to the manner in which the detection is performed: that is, by optical or electrochemical means. Fluorescence-based DNA microarrays, also known as “DNA chips” are the most widely known DNA sensors.[6] A key feature in their operating principle is that the DNA takes part in transducing the event recognized into an electrical read-out signal.[5] Most DNA microarrays rely on optical detection using fluorescent dyes, or, more recently, using quantum

dots. But the label attachment requires additional sample preparation and also increases the cost of the analysis.

Electrochemical detection has gained a significant amount of attention recently and has proven to be a promising alternative to more traditional optical detection methods. Electrochemical biosensors are able to convert the DNA hybridization event more directly into an analytical signal to acquire sequence specific information.[5,7,8] In general, these sensors consist of a solid electrode and a probe which is immobilized on the surface. Upon hybridization with its target, the DNA sensor produces an electrochemically detectable signal[9] as illustrated in Figure 1.1. The probe or the target DNA is tagged with a redox label that generates the signal. Electrochemical biosensors have potential advantages such as low cost, high sensitivity, simple designs and small dimensions.[7,10,11] Electro-active indicators such as ferrocene, cationic metal complexes as well as enzymes can be used to label the DNA. In the case of label-free electrochemical detection, detection is based on properties such as the capacitance of electrode-solution interface.[12]

In optically detected DNA hybridization, methods such as fluorescence, surface plasmon resonance, surface enhanced Raman scattering (SERS) and chemiluminescence are used. DNA microarrays are made either from glass, plastic or silicon and consist of 10-10,000 microspots. In optical detection using fluorescence, when the target DNA is fluorescently labeled, its hybridization with the probe is easily measured with the use of imaging fluorescence apparatus.[1] Interest in fluorescence based optical detection is mostly used due to its high sensitivity.[1] The primary focus of this thesis is in the area of fluorescence based detection of DNA hybridization.

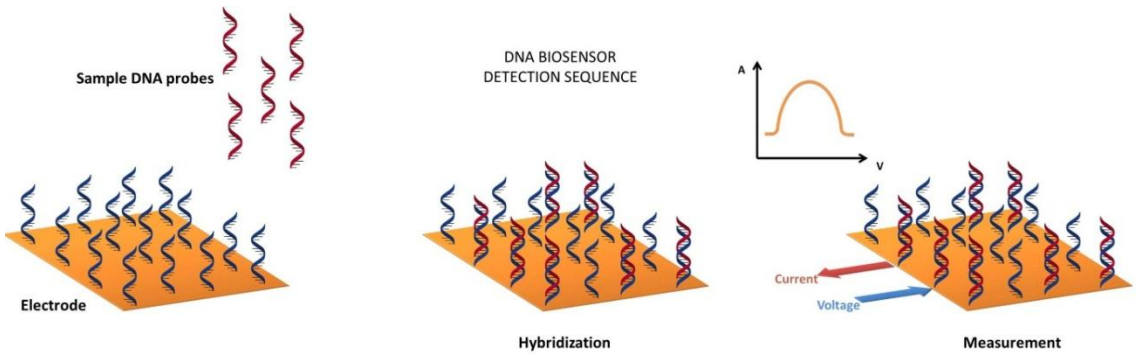

Figure 1.1 Perfect match between the probe DNA and its complementary target leading to a detectable read-out signal.

1.1.2 Field-induced DNA reorientation

Other than providing electrochemical means for DNA detection, the modulation of the electropotential during an analysis can be used to attract free target DNA and repel mismatched target. This in turn speeds up probe-target hybridization as well as allows better discrimination of sequence mismatch.[6] Additional control over the DNA orientation, hybridization or molecular recognition properties on surfaces is advantageous. As mentioned previously, such controlled manipulations aid in applications in DNA sensors. Many studies of electric-field induced DNA dynamics have been reported in the literature.[14,19,23] Rant, et al., were able to induce oligonucleotide reorientation electrically while probing the orientation of the electrode-bound oligonucleotides using optical techniques.[14] Studies related to the dependence of the dynamics on ionic strength, field modulation frequency, temperature and electric-field strength have been reported by many groups.[14,19,23] These studies show that the reorientation was limited at high frequencies by double layer charging. The dynamics were clearly shown to depend on the ionic strength of the solution. At high ionic strength, the DNA conformations were independent of the applied electric field. At low ionic strength, single strand DNA (ss-DNA) could be manipulated by electric fields due to a change in its structural properties (i.e., stiffness) or persistence length. The temperature dependence of both ss- and ds-DNA took different forms at low ionic strength. At high ionic strength, both were insensitive to temperature changes. The ds-DNA was able to maintain its structure up to the duplex melting temperature, whereas ss-DNA conformation showed a considerable change with temperature.

Kelley and co-workers were the first to prove that orientation of electrode bound DNA could be controlled by using electrochemical potentials at a metal electrode.[15] They used electrochemical atomic force microscopy (EC-AFM) to investigate layers of 15-mer ds-DNA attached to gold electrodes. The electrical potential of the working electrode, which supports the DNA monolayer, was modulated to study structural changes in the DNA layer as a function of the applied electric field. They observed that the orientation of both ss- and ds-DNA oligonucleotides attached to metal surfaces could be manipulated by changing the electrode potential. Depending on the applied electric field, a significant change in the film thickness was observed. Since the DNA backbone is negatively charged, positive surface charge attracts the

DNA strands. Hence, they tilt towards the electrode surface at applied positive potentials (vs. open circuit potential, OCP). In contrast, negatively biased electrodes (vs. OCP) repel the charged DNA strands so that they align perpendicular with respect to the electrode surface.[13,14] Figure 1.2 shows the DNA monolayer thickness as a function of working electrode potential measured by EC-AFM. The observation corresponds to a change in the surface topographic height. Switching between positive and negative potentials resulted in the formation of thin and thick monolayers respectively where the strands either stand up for the applied negative potential or lie down on the surface under an applied positive potential. While this work provides valuable evidence of potential-dependent DNA orientation, no information on reorientation dynamics was obtained in their work.[15]

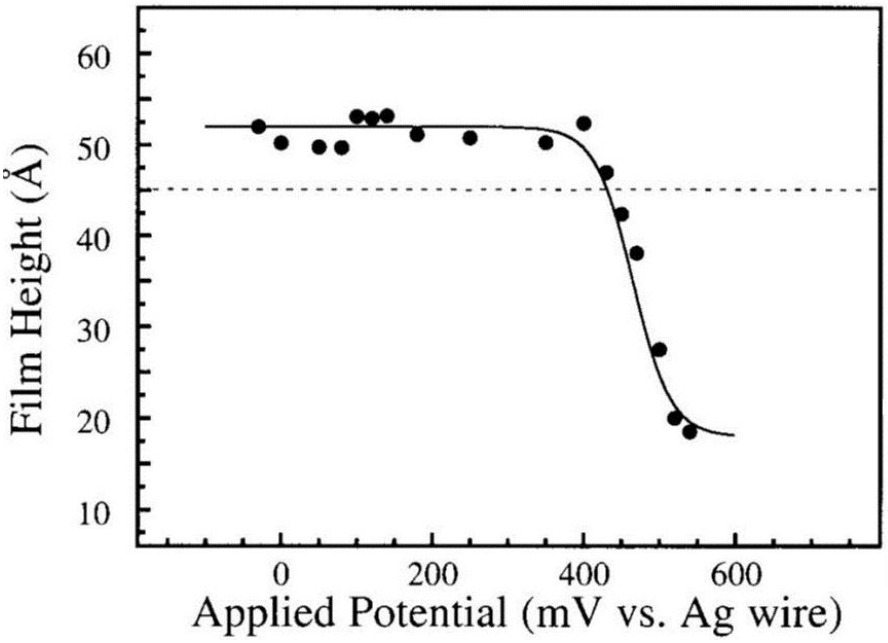

Figure 1.2 Potential dependence of monolayer thickness measured by atomic force microscopy under electrochemical control. The dashed line corresponds to the open-circuit value. Reprinted with permission from ref 15. Copyright 1998 American Chemical Society.

Heller and co-workers showed that electric fields can be used to control hybridization and denaturation of both ss- and ds-DNA.[16] They were able to show that by a simple adjustment of the electric field, discrimination between oligonucleotide hybrids with varying binding strengths could be obtained. Hence, with this approach, control of the electric field denaturation allowed for discrimination of matched and single-base-pair-mismatched DNA. DNA was not

immobilized on the electrode in these studies. They concluded that the electric field alone was not solely responsible for hybridization but that the dynamics may also be due to joule heating. They also suggested that the observed electric-field-induced dehybridization resulted from a reduction in the stability of the hybrid due to local pH changes.[16]

Field-enhanced hybridization/dehybridization of surface bound DNA on gold electrode surfaces was first investigated using in situ optical SPR methods by Heaton and co-workers.[17] They showed that electrostatic fields can cause the rate of hybridization of unlabeled DNA tethered to gold electrode surfaces to increase. They also demonstrated enhanced mismatch discrimination of hybrids by adjusting the electrode potential. Repulsive potentials caused denaturation in mismatched hybrids in a short period of time, leaving the complementary, matched hybrids unchanged. But no account for the role of field induced dynamics was made.[17]

Hairpins play a significant role in many biological functions. The primary difference between a hairpin structure and its related linear structure stems from the folding-unfolding manner of the hairpin. These possess a stem-and-loop structure where the loop portion is complementary to the target while the stem is self-complementary. Wei and coworkers used the so-called scanning potential hairpin dissociation (SPHD) method to investigate the dissociation of specially designed hairpins which were immobilized on silicon wafer surfaces and observed a decrease in the fluorescence intensity (from +0.5 V to -1.5 V),[18] as illustrated in Figure 1.3. They explored the influence of the stem length in the hairpin probe on the SPHD curve. Their study was based on a different mechanism involving labeling, measuring condition and the process involved. In labeling, Wei, et al., used Pico Green which is a ds-DNA specific intercalating dye and used a probe-functionalized silicon electrode in target solution during SPHD measurement. They concluded that when hairpin DNA denaturation was driven by slowly scanned electric potentials, the system reaches equilibrium for both the electric field distribution and the dissociation process.

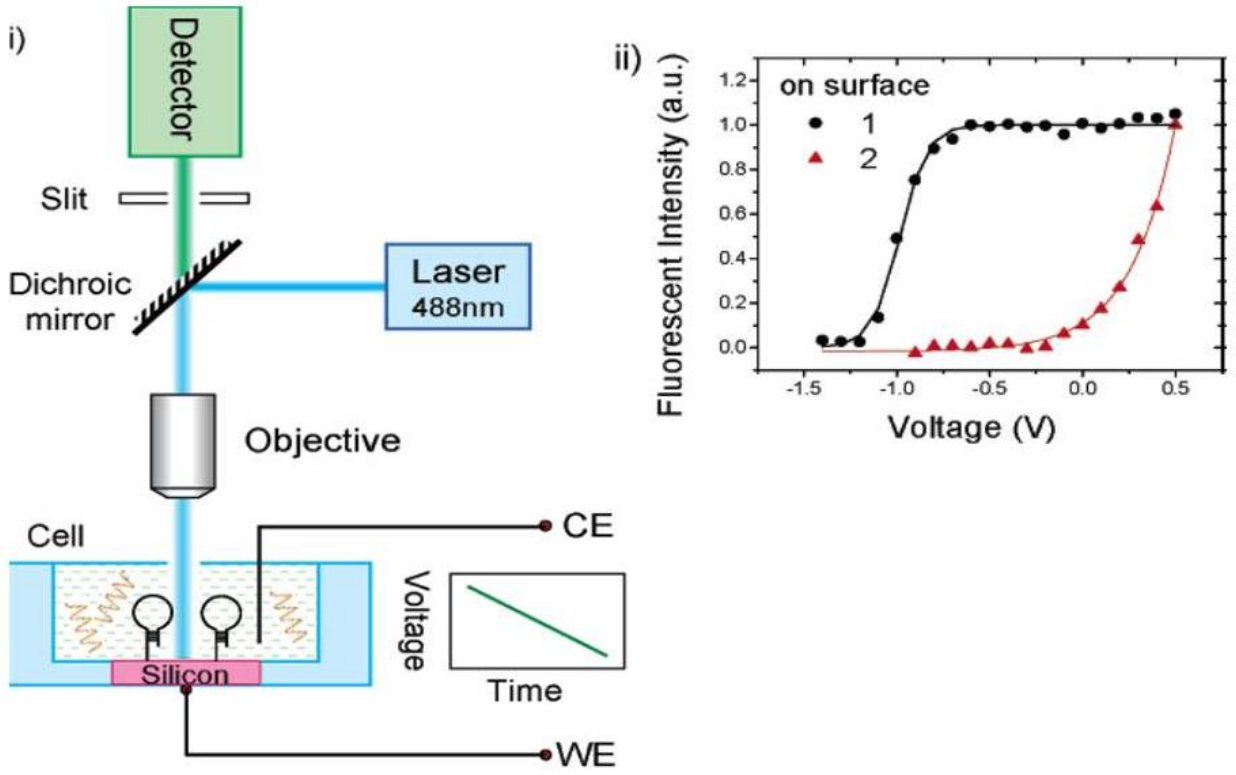

Figure 1.3 Schematic diagram of SPHD and the results obtained. (i) The apparatus used for SPHD. (ii) The SPHD curve for duplex of HPm5 (hairpin with 5 base pairs) with (1) the complementary target and (2) non-complementary strand when focus was on the surface. Reprinted with permission from ref 18. Copyright 2006 American Chemical Society.

The previous studies largely looked at the equilibrated DNA conformational changes or orientational changes as a means to sense DNA hybridization. But the field-induced DNA dynamics at the electrode surfaces are expected to be more complicated as the DNA interacts with the electric field of the charged double layer and both of them change with potential and time.

Rant and coworkers have extensively studied the field-induced dynamics of DNA on gold electrodes. They employed potential dependent (i.e., distance dependent) fluorescence quenching methods to investigate the dynamics of dye labeled DNA on gold surfaces. The authors explained that the dynamics for DNA switching had remarkable consistency when electrochemical and surface functionalization conditions were chosen appropriately. Through the variation of the surface coverage and thus the steric interactions between nearby strands, their

system allowed the study of surface-attached DNA densities from well-separated to closely-packed DNA strands as indicated in Figure 1.4. By employing the system Rant developed, the complicated dynamics and interactions of polyelectrolytes at the liquid/metal interface can be addressed.[14,19,20]

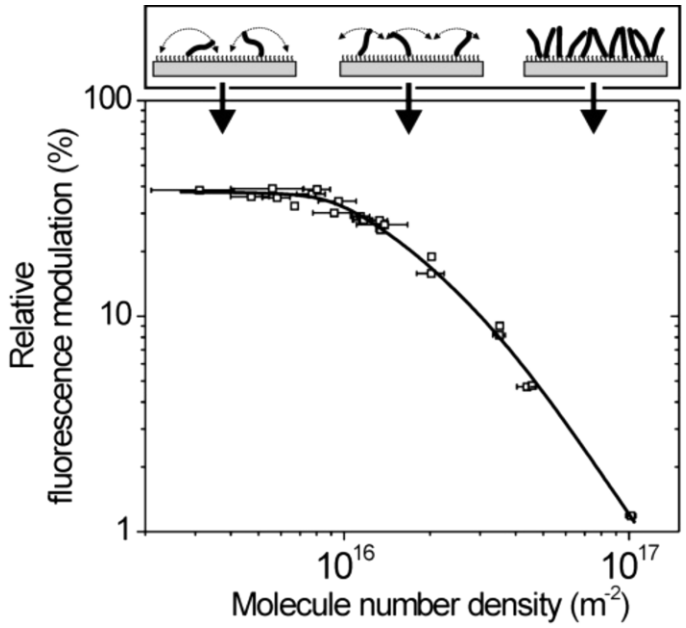

Figure 1.4 Influence of the packing density of molecules within layers of 24-mer ssDNA on the observable fluorescence modulation ($\Delta F/F_{avg}$). Reprinted with permission from ref 14. Copyright 2004 American Chemical Society.

Rant investigated the dependence of the DNA dynamics on salt concentration and field modulation frequency, using the amplitude of fluorescence modulation driven by square wave potentials as a means to monitor the dynamics.[21,22,23] DNA orientation was observed through the distance-dependent quenching of fluorescence from the dye, bound to the distal end of the DNA, to the electrode. It was observed that the presence of the strong electric field within the diffusive double layer is needed to produce changes in the DNA orientation.[14] They concluded that reorientation was limited at high frequencies by double layer charging. When the frequency is too high for the double layer to accrue, thermal fluctuations control the DNA orientation and its manipulation becomes impossible.

The overlap between the field and the DNA was also found to govern the dynamics. The DNA orientation was seen to be affected when only a small amount of its length was exposed to

the field and when the potential was modulated at frequencies up to the kHz level. At low frequencies (i.e., <10Hz), no changes in the dynamics were observed.[14,22] Rant, et al., were also able to show that dynamics differed under positive and negative potentials. When a positive potential was applied, it caused the fluorescent dye attached at the distal end to fold onto the electrode surface, whereas when a negative potential was applied it caused the fluorescent dye to extend away from the electrode surface. Bright fluorescence was observed for upright positions as illustrated in Figure 1.5.[14] With high salt concentrations the electric potential decays rather fast into the solution and a reduction in switching was observed. With a low salt concentration, maximum fluorescence switching amplitude was observed.

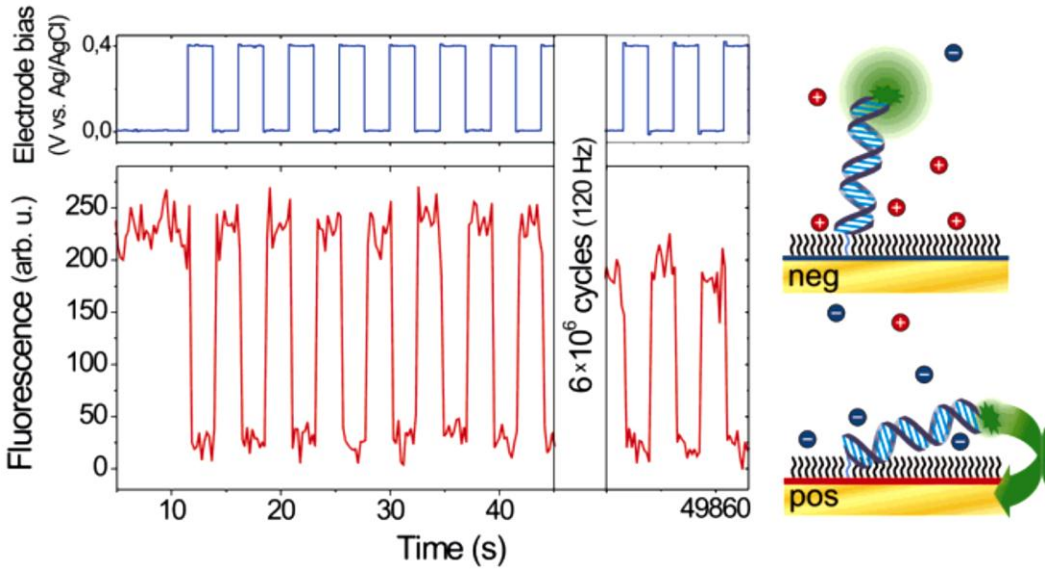

Figure 1.5 Dynamic electrical switching of DNA layers on a metal surface. Reprinted with permission from ref 14. Copyright 2004 American Chemical Society.

The dynamic response measured from a switchable ds-DNA layer taken by carrying out a frequency sweep of the AC potential applied to the gold electrode is shown in Figure 1.6. When the ss-DNA was exposed to its complementary strand in situ, a significant change in the switching behavior was observed. The fluorescence modulation amplitude showed a considerable increase upon hybridization, which is due to the distinct mechanical flexibilities of ss- and ds-DNA. The ds-DNA molecules behave as rigid rods and can be oriented efficiently by strong fields in the electrical double layer (EDL). In contrast ss-DNA behaves as flexible chains

that can only be partially aligned by strong electric fields.[19] As shown in Figure 1.6 the ds-DNA shows significantly enhanced switching in comparison to ss-DNA.

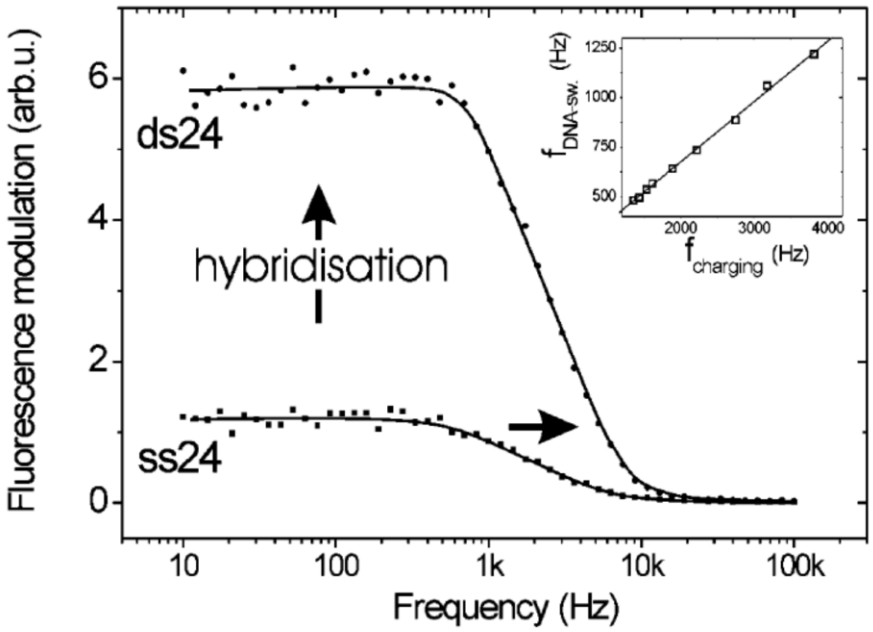

Figure 1.6 Response of the fluorescence modulation amplitude as a function of the frequency of the driving electrical AC potentials. Reprinted with permission from ref 14. Copyright 2004 American Chemical Society.

The studies described above have shown how surface bound DNA reorients under the influence of the double layer field and how the associated dynamics depend upon field strength and solution ionic strength. The authors of these studies mainly looked at DNA conformational and orientational changes as a means to sense DNA hybridization. They assumed that the ds-DNA played little or no role in EDL establishment.

1.1.3 Electrical double layer

When a charged surface is immersed in an electrolyte solution, a concentration gradient in the electrolyte develops forming the so-called EDL as shown in Figure 1.7. The potential profile associated with the EDL shown in Figure 1.8 illustrates how the surface charge potential changes with distance. Out of several theoretical treatments of the solid-liquid interface, the Helmholtz model, Gouy-Chapman model and Stern's modification of the double layer are given prominence. The Gouy-Chapman theory models a rigid charged surface, with a gathering of oppositely charged ions in solution near the surface. The concentration of the oppositely charged

ions decreases with distance from the surface. The resulting concentration gradient is known as the diffuse double layer.

The thickness of the EDL, which is defined by the Debye length λ_D, is given by:

$$\lambda_D^2 = \frac{\varepsilon\ \varepsilon_0\ k_B T}{2ne^2}$$

Here, ε is the relative permittivity of the solvent, ε_0 that of a vacuum, k_B is the Boltzmann constant, T is the temperature, n is the ion density and e is the charge of the electron.

In an electrolyte the Debye length is usually denoted by κ^{-1} and is given by:

$$\kappa^{-1} = \sqrt{\frac{\varepsilon\varepsilon_0 k_B T}{2N_A e^2 I}}$$

where I is the ionic strength and N_A is the Avogadro number. As shown through these equations, λ_D increases with decreasing ionic strength. Surface-bound oligonucleotides of short effective length that are similar to the Debye length encounter strong electric fields at the electrode surface, allowing control over the DNA orientation. Gouy-Chapman theory only strictly applies to the distribution of freely-mobile ions in solution. In the present studies, significant charge is bound to the electrode surface along the DNA strands. While the presence of these charges has been neglected in previous work, it is not clear such an assumption can be made. In that case the charges on the DNA may strongly perturb the double layer structure and dynamics. Understanding such perturbations is a primary long term goal of this project.

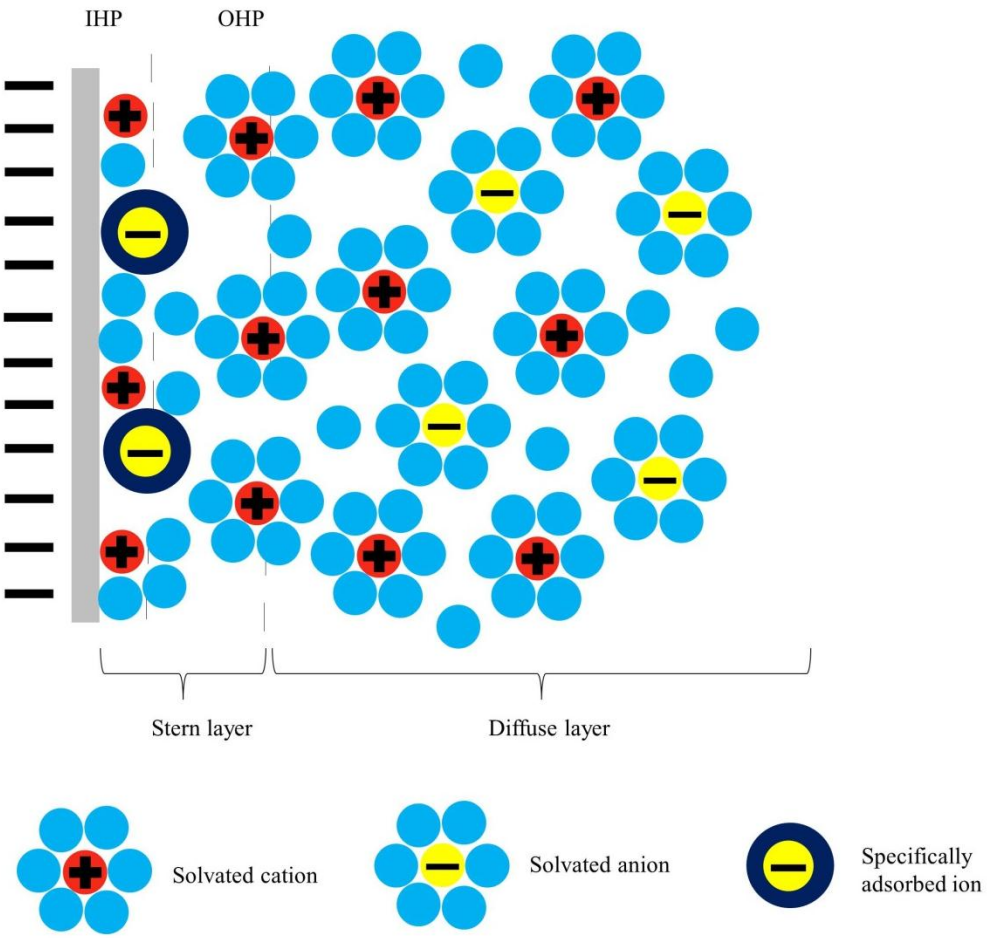

Figure 1.7 Electrical double layer.

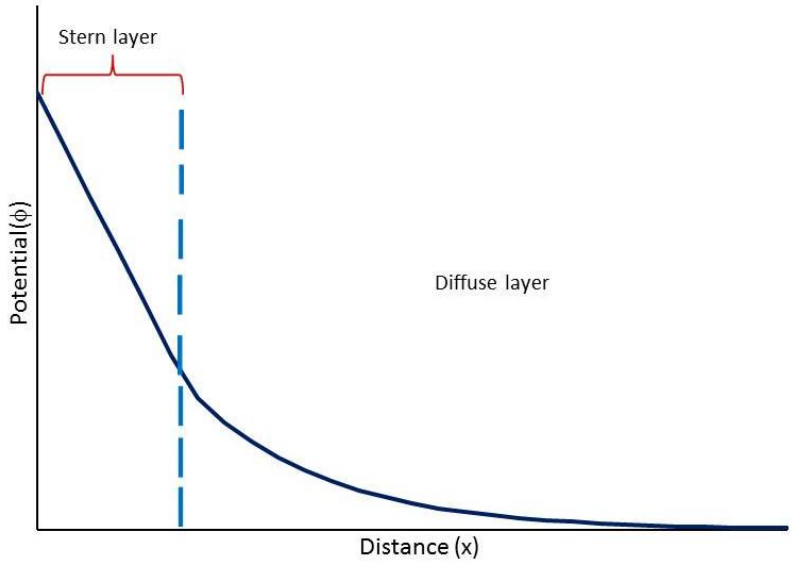

Figure 1.8 Potential profile at the electrical double layer.

1.1.4 Dipole-electrode quenching

The variation of fluorescence from the dye attached to the DNA during its reorientation is attributed to dipole-electrode energy transfer.[13] The rate constant for energy transfer, k_{et} is proportional to d^{-3} or d^{-4} where d is the distance between the dye and the surface. Here, the d^{-4} dependence has been adopted, as previously reported in the literature[13,24]:

$$k_{et} = \frac{1}{\tau}\left(\frac{d_0}{d}\right)^4$$

where τ is the fluorescence lifetime of the dye in the absence of energy transfer and d_0 is the quenching distance at which $k_{et} = 1/\tau$. Energy transfer competes with radiative as well as nonradiative deactivation of the photoexcited fluorescent dye. The quantum yield for energy transfer, ϕ_{et} is given by:

$$\Phi_{et} = \frac{k_{et}}{k_r + k_{nr} + k_{et}}$$

Combining these two equations and using the relationship $1/\tau = k_r + k_{nr}$ the expression for the quantum yield becomes:

$$\Phi_{et} = \frac{1}{1 + (d/d_0)^4}$$

Then, the ratio between fluorescence intensity at distance d and infinite distance from the electrode surface can be shown to be:

$$\frac{F_d}{F_\infty} = 1 - \Phi_{et} = \frac{1}{1 + (d_0/d)^4}$$

The value of d_0 is found using an equation from Jennings, et al.[24]:

$$d_0 = 0.225 \left(\frac{c^3 \phi_{dye}}{\omega_{dye}^2 \omega_F k_F}\right)^{1/4}$$

where the speed of light in a vacuum is given by c, ϕ_{dye} is the fluorescence quantum yield of the dye (0.8 for 6- carboxyfluorescein, FAM6),[13] ω_{dye} is the angular frequency of electronic absorption for the dye (3.65×10^{15} s^{-1}, ω_F is the Fermi frequency of the electrode (6.99×10^{15} s^{-1} for the glassy carbon electrode (GCE), derived from its work function, which is assumed to be

4.6 eV), and k_F is the Fermi wave vector for the GCE (1.10×10^8 cm^{-1}). The calculated value of d_0 is 8.30 nm.[13] This value is slightly larger than that for a similar dye interacting with gold nanoparticles (d_0 = 7.63 nm).[24]

1.2 Materials

1.2.1 Glassy carbon electrode

The previous studies described above almost exclusively used thiol modified DNA attached to gold electrode surfaces. However, it has been revealed that thiol linked DNA probes desorb at potentials more negative than -775 mV (vs. saturated calomel electrode, SCE)[25] and that thiols can be oxidized at potentials more positive than 600 mV (vs. SCE).[26] Hence, the useful potential window is limited for DNA bound to gold electrodes. Carbon electrodes are a promising alternative and offer advantages such as low cost, wider potential window, chemical stability and high electro-catalytic activity.[29,30] DNA is readily attached to the surface of carbon electrodes via the formation of an amide bond between –COOH groups on the electrode (produced by etching in a NaOH solution) and an amine linker on the DNA.[13,27] The strength of this amide bond to carbon (>300 kJ/mol) is relatively high in comparison to that of the gold-thiol bond (140-160 kJ/mol).[28]

Glassy carbon is a type of non-graphitic carbon that is commonly used as an electrode material.[29] The name "glassy carbon" originates from the fact that it exhibits a fracture behavior which is observable in glass. Glassy carbon is a hard and shiny material that can be easily polished. Even at high temperatures, glassy carbon cannot be converted into crystalline graphite and comprises a material of high thermal stability, high resistance towards chemical attack, high impermeability to gases and has the broadest potential range observed for carbon electrodes.[29,30] Early studies assumed that both sp^2 and sp^3 bonded atoms were present in the glassy carbon structure. Jenkins and Kawamura described an intertwined ribbon like structure.[31] Recently, based on results obtained by transmission electron microscopy, Harris brought forward a model that contains a structure which is associated with that of fullerene. The model shown in Figure 1.9 was proposed by Harris. This structure mainly consists of multilayered, broken or defective fullerene-like nanoparticles. The tightly packed microstructure explains the low reactivity of glassy carbon at low temperatures. Glassy carbon is an "amorphous" material with small graphitic domains: i.e., fullerene like nanoparticles that abruptly terminate at domain boundaries.

Because of the prevalence of these boundaries there are a large number of edge atoms on any surface. These edge atoms have high reactivity in comparison to the "in-plane" carbon atoms. At edge sites –COOH groups are readily formed upon oxidative etching of the glassy carbon.[31,32]

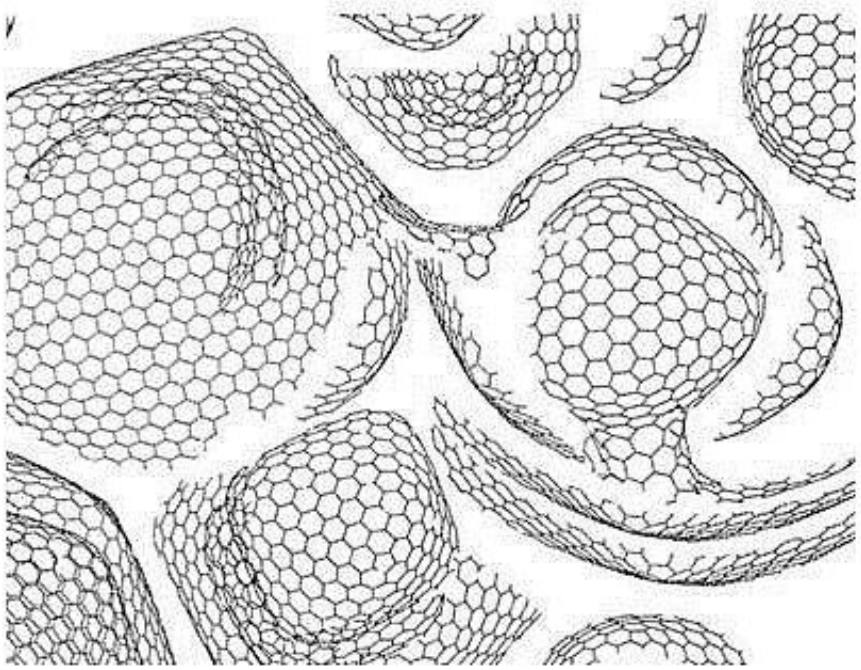

Figure 1.9 Model for the structure of high temperature glassy carbon containing fullerene like structures proposed by Harris. Modified from ref 31.

1.2.2 Structure of DNA

DNA is a linear chain of nucleotides, where each consists of a phosphate group, ribose sugar and a heterocyclic nitrogen base. Information is encoded in the sequence of the four bases: thymine (T), cytosine (C), guanine (G) and adenine (A). These four bases are divided into two classes, purine bases (adenine and guanine) and pyrimidine bases (thymine and cytosine). These bases are complementary, meaning hybridization occurs between two ss-DNA strands through specific pairing of the bases (A-T) or (G-C) by hydrogen bonding interactions. This specific pairing results in the formation of a helical structure of the ds-DNA, the Watson-Crick double helix.[33] Figure 1.10 shows the structure of ds-DNA illustrating the base pairing. While the

phosphate groups form the backbone of the DNA structure, the base pairs are localized inside the helix. Under physiological conditions, the phosphate groups are ionized, with each phosphate group carrying a negative charge. Counter cations (not shown) also incorporate within the double helix, compensating for at least some of the negative charges.

The persistence length of a DNA strand is a basic mechanical property which quantifies its flexibility.[34] Knowledge of the value of the persistence length is important for analysis of biochemical processes involving interactions of DNA strands. DNA persistence length is dependent on ionic strength as well as the DNA sequence.[35] Under common buffer conditions (i.e., 1X phosphate buffered saline, 1X PBS) the persistence length of ds-DNA has been measured to be ~ 50 nm. The persistence length of ss-DNA is much shorter (i.e., 2 nm).[36,37]

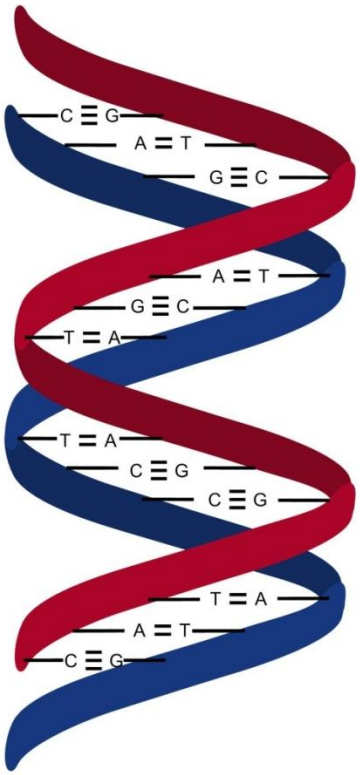

Figure 1.10 Structure of DNA.

1.3 Wide-field fluorescence microscopy

Fluorescence is a highly sensitive method for detecting the presence of certain types of molecules such as fluorophores and, under appropriate conditions, their dynamics over a range of time scales. Fluorescence is a three step process. The process responsible for the fluorescence of fluorophores can be illustrated by a simple electronic-state diagram as shown in Figure 1.11.

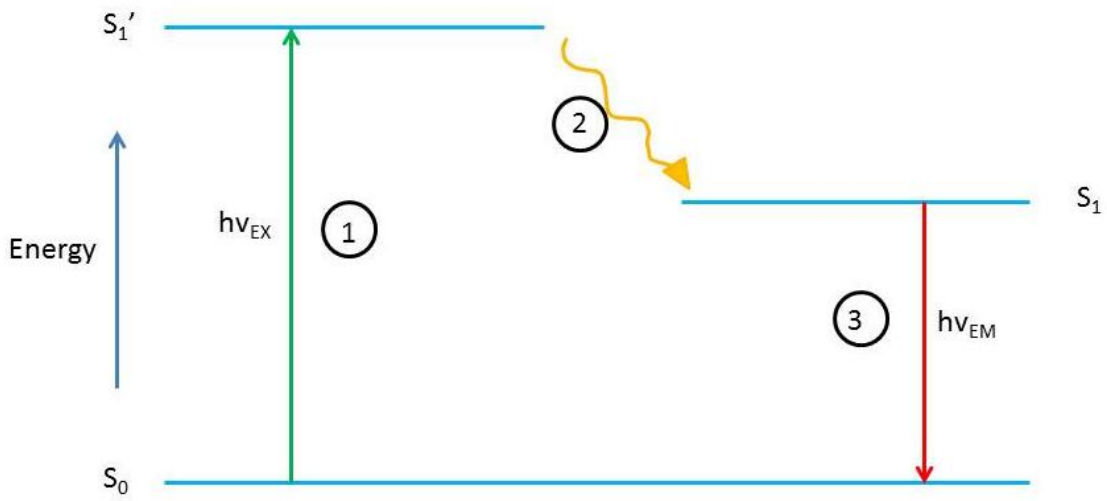

Figure 1.11 The electronic-state diagram for the fluorescence process.

Three stages of the electronic process leading to fluorescence are shown in the diagram. As indicated in stage 1, when a photon having an energy hv_{EX} is supplied externally via a light source such as a laser, the fluorophore absorbs this energy and an excited electronic singlet state (S_1') is created. The excited-state exists only for a short time (~1-10 ns) during which the fluorophore may undergo conformational changes as well as various interactions with the molecular environment. This leads to stage 2 in which some of the energy of the excited electronic state is dissipated, yielding a relaxed singlet state (S_1). In stage 3, the fluorophore returns to its ground state from the relaxed S_1 state by emitting a photon of energy hv_{EM}. Due to energy dissipation during the excited-state lifetime, the energy of this photon is lower than that of the absorbed photon. The fluorescence process is cyclical. Unless photobleaching occurs, the same fluorophore can be excited and detected repeatedly. The fact that a single fluorophore can produce a number of detectable photons is important to the high sensitivity of the fluorescence detection method.[38]

Fluorescence from dye labeled DNA attached to an electrode surface is very weak due to quenching to the electrode. To overcome this difficulty, we use a microscope with a high numerical aperture (NA) objective to both excite the fluorophores and collect their luminescence. The high NA objective provides the high collection efficiency required to detect extremely low light levels. The use of a microscope also allows us to look at whether dynamics are homogeneous or not.

Figure 1.12 shows a schematic of the wide-field fluorescence microscope employed in this thesis. The typical components required for a fluorescence microscope are a light source, objective, an excitation filter, a dichroic mirror and an emission filter. The dichroic mirrors and the filters are chosen to match the spectral excitation and emission characteristics of the flurophore used to label the specimen of interest. Out of all these optics, the most important component of an optical microscope is the objective. The objective is responsible for collecting the primary image of the sample and also plays a vital role in determining the quality of the magnified image produced. The objective used in an optical set up must be able to provide excellent light collection abilities and to provide good lateral and depth resolution as well. The collection efficiency of an objective lens depends on the NA of the objective. NA is related to the lens power. When NA is greater, the resolving power of the lens would be better. The light gathering power of a lens is also improved with increasing NA. Although we do have to use intense laser power which in turn may lead to photo bleaching, compared to the optical fiber system Rant, et al. used in their work,[14] we assume that the collection efficiency we can obtain in our system is much higher.

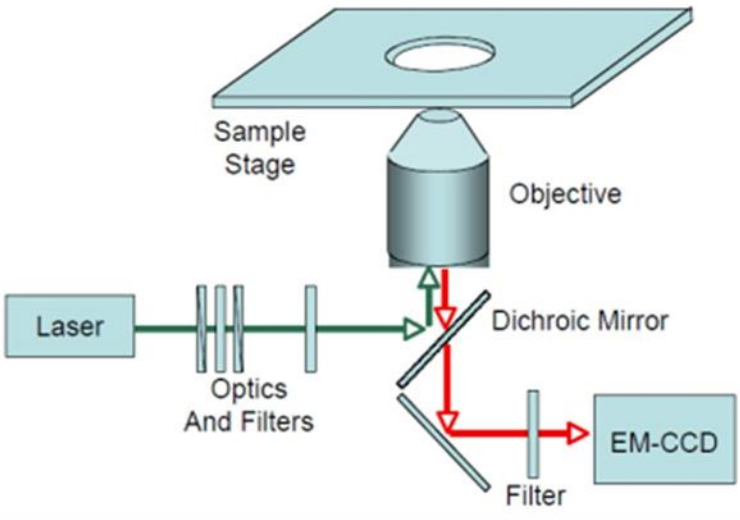

Figure 1.12 A diagram of a wide-field fluorescence microscope.

1.4 Motivation of these studies

It has been shown in many previous studies that applied electric fields can be used to induce reorientation of dye labeled DNA attached to a gold electrode surface. DNA dynamics in these studies were detected by monitoring the fluorescence of the dye labeled DNA and its quenching to the electrode surface. Work in this thesis is also focused on investigating the dependence of the DNA reorientation dynamics on surface coverage. In recent work by Qin Li and coworkers,[13] it was shown that new DNA reorientation dynamics were observed for DNA attached to glassy carbon electrodes. These dynamics were attributed to slow relaxation of the DNA following a potential step. While these results were attributed to previously unobserved orientational relaxation, there were concerns that pH changes at the electrode surface may contribute and that the cell geometry could be a limiting factor. This thesis seeks to eliminate these possibilities by use of a new cell design and by use of better buffer.

The subsequent chapters of this thesis describe the experiments performed, in detail. Chapter 2 provides experimental details on preparing the DNA modified GCE, electrochemical cell preparation and optical detection of the DNA switching. Chapter 3 gives results and discussion of these studies on the observed signal switching, the trend observed in the reorientation time constant with increasing probe concentration at applied positive and negative biases and the possible reasons for the observations. Finally, Chapter 4 presents the conclusions and future work.

Chapter 2 Experimental Details

2.1 Materials

DNA oligonucleotides were purchased from IDT (Integrated DNA Technologies). A 35-mer oligonucleotide probe (P), along with its complementary target (T) were used. Their sequences are as follows:

P: FAM6-5′-TGTGCTTTGTTCTGGATTTCGCAGGTCCTCAAGGG -3'-aminoC6dT
T: 3'-ACACGAAACAAGACCTAAAGCGTCCAGGAGTTCCC-5'

We used a genomic DNA sample that contained a representative BRCA 1 (breast cancer 1, early onset) gene SNP (single nucleotide polymorphism). The gene sequence was obtained from GenBank. BRCA 1 is a tumor suppressor gene which is associated with the occurrence of breast cancer as well as several other cancers.[39] The sequence ACCTGCGAAAT is a part of a BRCA 1 gene sequence. The underlined base (C) represents a single base that is mutated to T in cancer patients, a so called SNP. This specific BRCA 1 gene mutation is at Arg1443ter in exon13, codon1443. The length of the 35-mer DNA strand employed (see P) was determined using an internet tool[40] and was estimated to be 11.55 nm.

Figure 2.1 shows the structure of the fluorescent dye, FAM6, which is covalently attached to the 35-mer oligonucleotide probe. The AminoC6dT designation symbolizes a standard linker -NH-CH_2-CH_2-CH_2-CH_2 -CH_2-CH_2-NH_2, which was incorporated by the vendor. The amino modified DNA is end grafted to the -COOH on the glassy carbon electrode surface by amide bond formation. The six carbon linker allows for better attachment to the surface by increasing molecular flexibility.

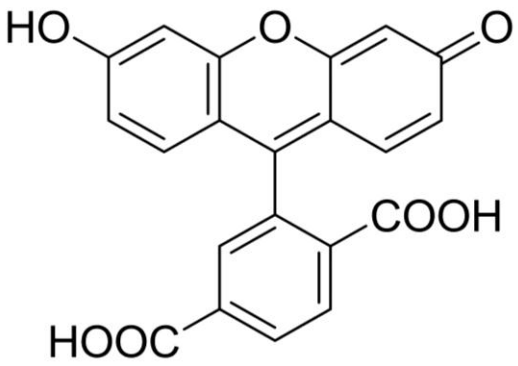

Figure 2.1 Structure of FAM6

2.2 Preparation of DNA modified electrodes

2.2.1 Glassy carbon electrodes

Glassy carbon chips with dimensions of 17 mm x 15 mm x 2 mm were used as electrodes and were obtained from SPI Supplies. In conditioning these electrodes for DNA attachment, they were first rinsed with ethanol and polished for 5 min using 0.05 μm gamma alumina slurry (Buehler) on napless polishing cloth. This was followed by washing and sonicating the GCE in deionized water for about 15 min. Surface contaminants were removed from the electrode in this process and more active edge planes were obtained. Polishing is a common step in the preparation of carbon electrodes in electrochemistry. It is a good practice to sonicate after polishing, but the purity of the sonication liquid is important. Sonication will remove the particles but at the same time allow adsorption of contaminants from the sonication bath. After sonication, the electrodes were electrochemically activated by etching in a 1.0 M NaOH solution. For this purpose, the electrode potential was stepped between -0.1 V and 1.2 V (vs. SCE). This final procedure produced an abundance of –COOH groups on the GCE surface for attachment of DNA by formation of an amide bond to the electrode surface (see Figure 2.2).

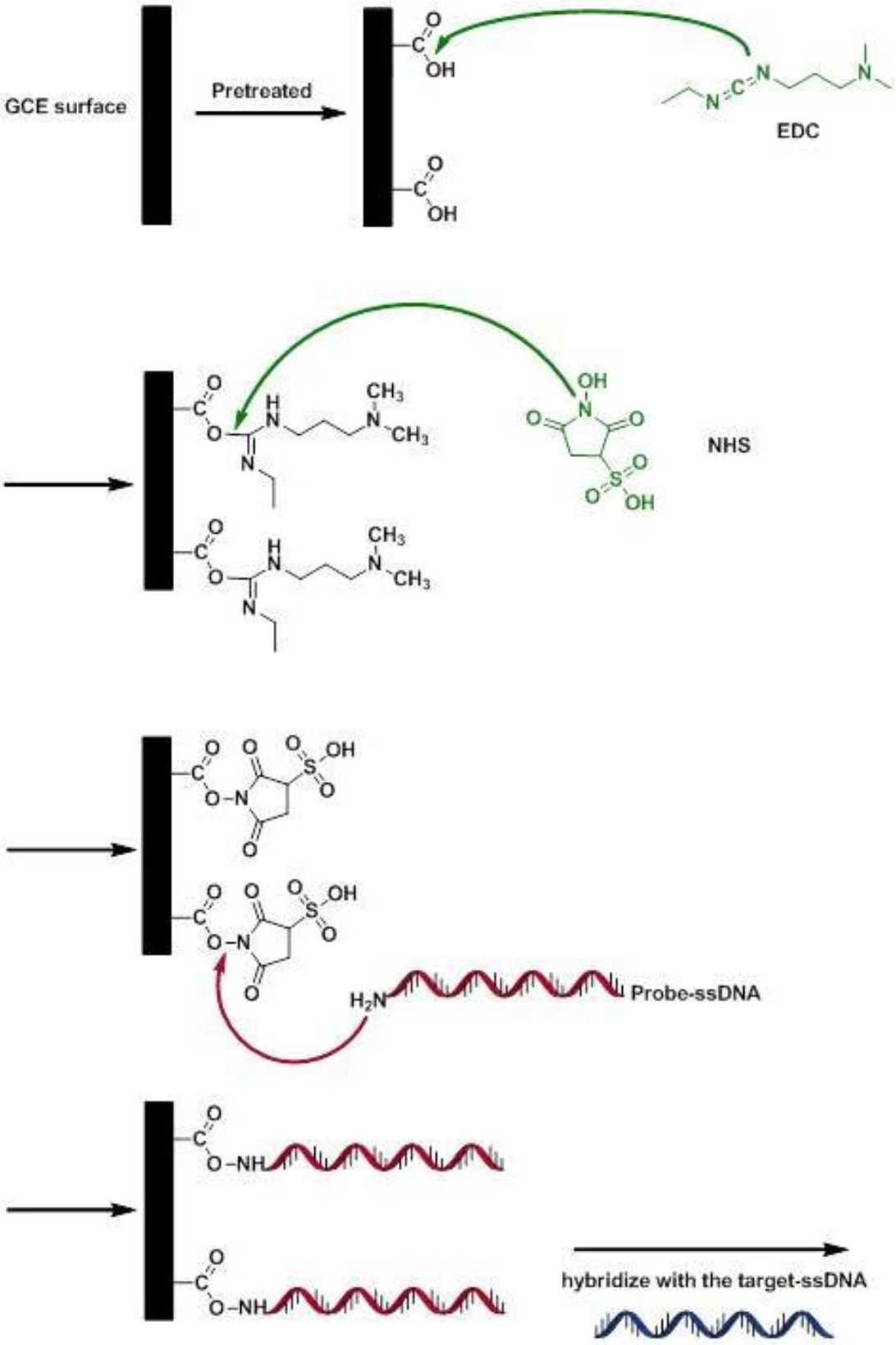

Figure 2.2 Scheme for preparation of DNA modified electrodes.

2.2.2 DNA functionalization

The amine modified DNA was end grafted onto –COOH groups on the GCE surface. During this step, the GCE was incubated with 50 µL of 0.25, 1.0 and 1.5 µM buffered DNA in 1X PBS solution (pH 7.4) (137 mM NaCl, 2.7 mM KCl, 8.1 mM Na2HPO4•H2O, and 1.76 mM KH2PO4). This procedure was carried out in the presence of 1-ethyl-3-[3-dimethylaminopropyl] carbodiimide hydrochloride (EDC) (25 mM) and N-hydroxysulfosuccinimide (NHS) (10mM) catalysts. The reaction was run at a temperature of 40 ºC for 2 hours. Figure 2.2 provides a schematic view of the functionalization reaction.

2.2.3 Electrode passivation

After DNA functionalization, the remaining active sites on the electrode surface were passivated by immersing the electrode in 1.0 mM hexylamine solution with the same catalysts as in the previous step. The passivation step serves to cap any remaining active sites on the GCE surface.

2.2.4 DNA hybridization

DNA hybridization was achieved by incubating the modified electrodes in 50 µL of 5.0 µM complementary target solution in 2X saline sodium citrate (SSC) buffer (0.3 M NaCl and 30 mM trisodium citrate, pH 7.0) for 2 hours. The temperature was maintained at 55 ºC in this step. After incubation, the DNA modified electrode was slowly cooled to room temperature, in the dark.

Each step was followed by washing with 1X PBS and 20X SSC buffer solutions. The DNA modified glassy carbon electrodes were stored in 20X SSC buffer solution at 4 ºC until they were used. Figure 2.3 shows the hybridization chamber used in DNA functionalization and hybridization, while Figure 2.4 shows the incubator.

Figure 2.3 Hybridization chamber used in DNA functionalization and hybridization.

Figure 2.4 Incubator used in DNA functionalization and hybridization.

2.2.5 Surface density of DNA

The surface density of DNA was measured for varying surface coverages by electrochemical methods. DNA modified surfaces were prepared using the previously described procedure (see section 2.2). Different surface coverages were obtained by changing the DNA probe concentration in the functionalization bath. Concentrations of 0.25, 1.0 and 1.5 μM were employed.

The electrochemical method employed to quantify the surface density of DNA immobilized on GCE was originally developed by Steel and co-workers.[41] In this method, DNA modified electrodes are exposed to 50 μM hexammineruthenium(III) chloride in 10 mM Tris-HCl buffer. Electrochemical characterization of the DNA surface density was performed in a large Teflon cell. The working electrode was the modified GCE, a Ag/AgCl (4 M KCl) electrode served as the reference and a Pt wire as the counter electrode in the three electrode set-up. The modified GCE was sealed against the cell using an O-ring with an inner diameter of 3.0 mm (see Figure 2.5). Thus, only an area of about 0.071 cm^2 on the GCE was exposed to the solution. Approximately 500-600 μL of the electrolyte solution was used to fill the cell. The oxygen in the electrolyte solution was removed by purging the electrolyte with nitrogen for 15 min.

DNA density was quantified using chronocoulometry by calculating the saturated amount of charge-compensating redox-marker, hexammineruthenium(III)chloride, in the DNA monolayer. The saturated amount of $Ru(NH_3)_6^{3+}$ is directly proportional to the amount of phosphate residues and hence to the surface density of DNA. In measuring this charge, the potential was switched from +0.2 V to -0.3 V. The latter was beyond the cathodic peak observed for Ru^{3+} reduction in cyclic voltammograms. The potential was held at -0.3 V for 1 second or more while the charge was recorded. As Ru^{3+} undergoes one-electron reduction, the charge passed provides a direct measure of the bound Ru^{3+} concentration, which directly yields the phosphate concentration after accounting for the factor of 3 binding stoichiometry. The same experiment was carried out for a blank 10 mM Tris-HCl buffer to find the amount of adsorbed $Ru(NH_3)_6^{3+}$ and hence, the surface density of DNA.

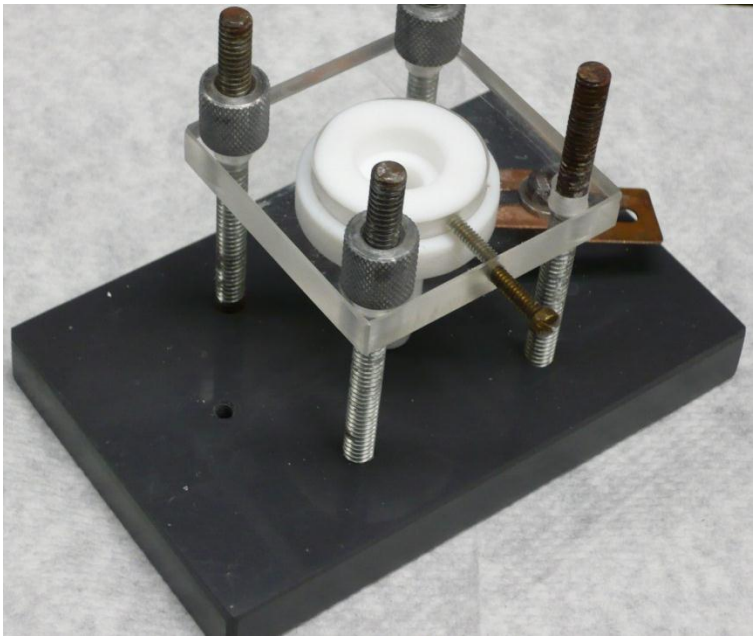

Figure 2.5 Teflon cell used in surface density experiments.

2.3 Preparation of the electrochemical cell

DNA switching experiments were carried out in a custom made electrochemical cell. The counter and reference electrodes were fabricated on an ITO (indium tin oxide) coated cover glass with dimensions of 22 mm X 26 mm, as shown in Figure 2.6. The ITO was patterned by photolithography, as described in the following section. The area designated as the counter electrode was coated with platinum using an ion beam coater. The Ag quasi reference electrode was fabricated by casting silver epoxy on the ITO pad. Copper wires were attached on either side of the patterned glass with the use of conductive silver epoxy.

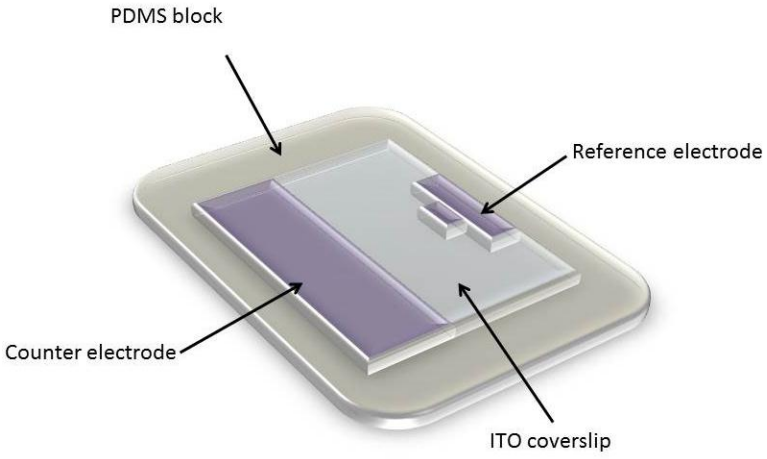

Figure 2.6 Schematic of the electrochemical cell.

2.3.1 Photolithography process

Positive tone lithography was employed in patterning the ITO cover glass with the desired pattern. Firstly, the cover glass was thoroughly cleaned with acetone and rinsed with isopropyl alcohol (IPA) to remove any contaminants from the surface. This step was followed by blow drying of the glass with N_2. The cover glass was then placed on the wafer holder (glass petri dish) and dehydrated for 1 min on a hotplate that had been preheated to a temperature of 65 ºC. Dehydration baking ensures that most H_2O on the sample evaporates prior to use. Otherwise, oxides will bond to a water layer and when the photoresist layer is coated on the sample, the photoresist layer will adhere to the water instead of the sample, as shown in Figure 2.7.

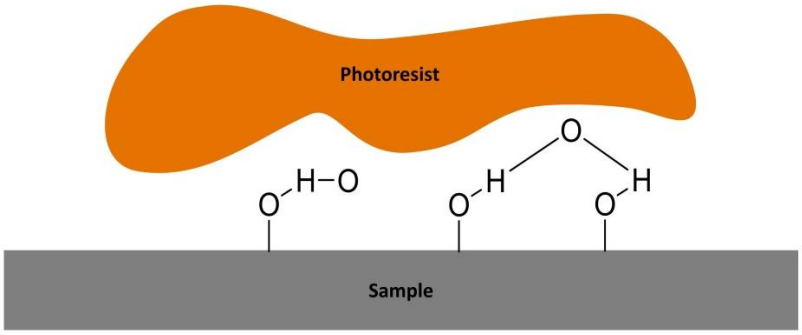

Figure 2.7 Chemistry during the dehydration baking.

After letting the cover glass cool down to room temperature, it was mounted on a spin coater and a primer coat was applied (200 µL MCC Primer 80/20) followed by a photoresist (240 µL of Shipley1813). The cover glass was then spun for 40 s at a speed of 1500 rpm with low acceleration, between each coat, in order to obtain a thin uniform layer of photoresist on the surface of the glass. It is important to make sure that the sample is not coated with an excess amount of the primer as it will reduce the photosensitivity of the photoresist. Spin coating produces a constant thickness of the photoresist on the sample. The cover glass was then placed on the wafer holder and baked for 15 min at a temperature of 115 ºC. This baking is known as a "soft bake", by which the volatile solvents are removed from the coating. Over baking the sample will lead to an increase in the sensitivity to UV light and may destroy the photoactive component, which will result in reduced solubility of the photoresist in the developer.

Next, the photoresist-coated ITO was placed on the mask aligner and suction was applied through a vacuum. After placing the mask with the desired pattern on the ITO cover glass, the

ITO was exposed to UV light (250 W) for a time period of 50 s. The areas which are exposed to the UV light will undergo a chemical reaction. By keeping the mask as close as possible to the sample, diffraction of light in the gap between the sample and the mask is avoided, improving the resolution of features produced. Avoid looking at the UV light directly while exposing the ITO cover glass. See Figure 2.8 for a schematic showing the full lithographic process.

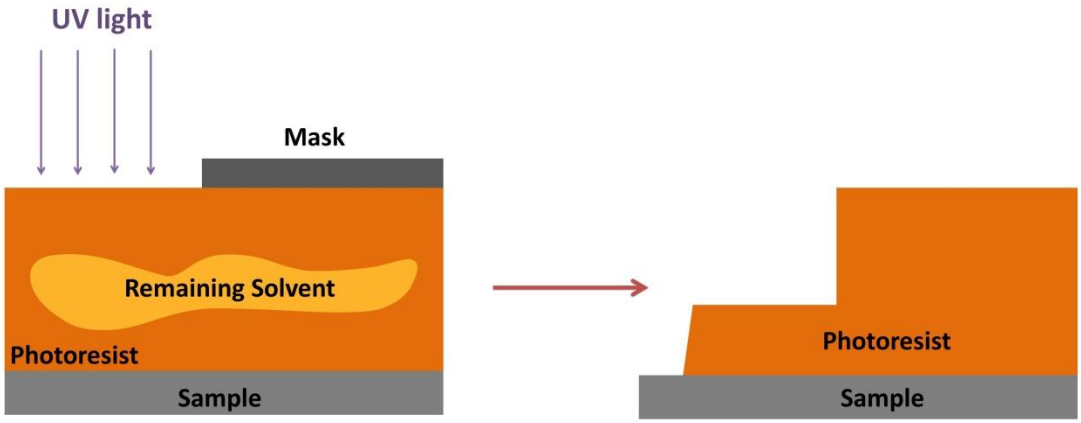

Figure 2.8 Sample exposure to UV light.

After exposure to UV light, the cover glass was then rinsed with developer (Microposit 351 Developer: water = 1:5), rinsed with deionized water, blow dried and dehydrated at 105 ºC for 20 min. Through rinsing with the developer, the UV exposed region of the photoresist is removed. Hard baking of the sample at this point is important as it will strengthen the remaining photoresist and improve bonding between the cover glass and the photoresist. This is an important step to perform before etching the sample to make sure that the photoresist will not be removed by the etching. After developing the ITO sample, the remaining photoresist will have a profile that looks like the structure shown in Figure 2.9.

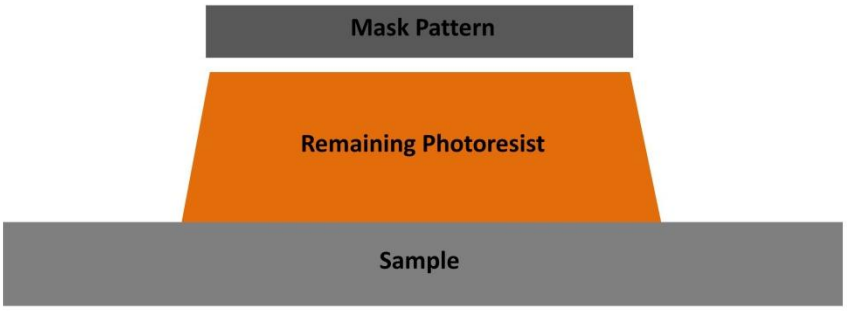

Figure 2.9 Profile of the photoresist after developing the sample.

Next, the ITO cover glass was immersed in an etching solution (10% $^{v}/_{v}$ HNO_3 with 40% $^{v}/_{v}$ HCl) to produce the desired electrode pattern. Etching was performed at a temperature of 50 ^{o}C for about 10-15 min and was terminated when the conductivity was lost in the etched regions. Finally, the ITO cover glass was washed with acetone, isopropyl alcohol and then by deionized water to remove the photoresist. It was then blow dried and dehydrated for 5 min at a temperature of 65 ^{o}C. Figure 2.6 shows a typical diagram of the final pattern obtained after the photolithography process.

2.3.2 Assembling the electrochemical cell

As shown in Figure 2.10, the cell-body is constructed by pasting a polydimethylsiloxane (PDMS) block of 6 mm thickness on the patterned cover glass. To form the internal cell volume, a square piece of the PDMS was cut and removed from the middle of the PDMS block. Then two spacers, each with a thickness of 0.3 mm were glued to the cover glass to form the open cell volume. The glassy carbon working electrode was placed on top of these spacers. Using a holder as shown in Figure 2.11, the GCE was clamped down. Electrical connections were made using alligator clips to connect with the appropriate electrode connections of the potentiostat. Figure 2.12 shows the cell after final assembly.

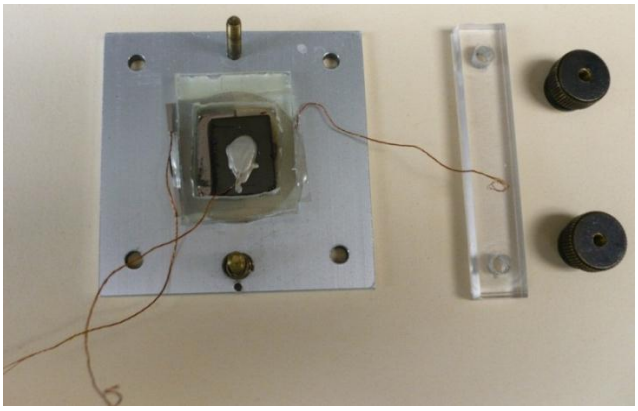

Figure 2.10 Cell placed on the holder.

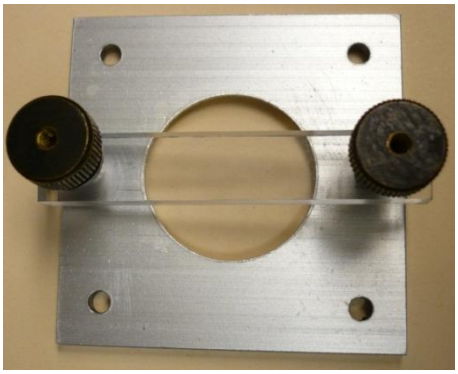

Figure 2.11 Holder used to keep the GCE clamped down.

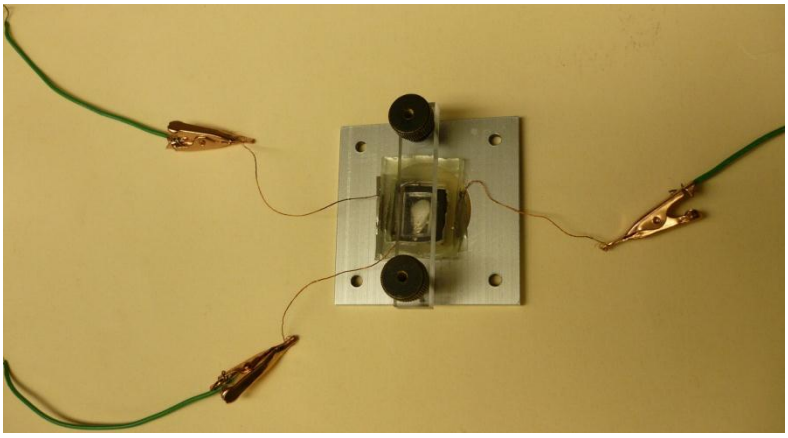

Figure 2.12 Cell after the final assembly.

2.4 Instrumentation

2.4.1 Electrochemistry experiment

Electrochemistry measurements were performed using a potentiostat (CH Instruments, Inc) (see Figure 2.13) and the electrochemical cell described in Figure 2.12. In both fluorescence and electrochemical experiments the glassy carbon electrode served as the working electrode, which was placed on top of the spacers in the PDMS chamber. The cell chamber was filled with buffer solution using a syringe. A square wave form of 10 steps with a step width of 2 s was typically applied to the glassy carbon electrode. A potential range of -0.4 V and 0.2 V relative to the open circuit potential was commonly employed (see Figure 2.14).

Figure 2.13 CH instrument used in the electrochemistry experiment.

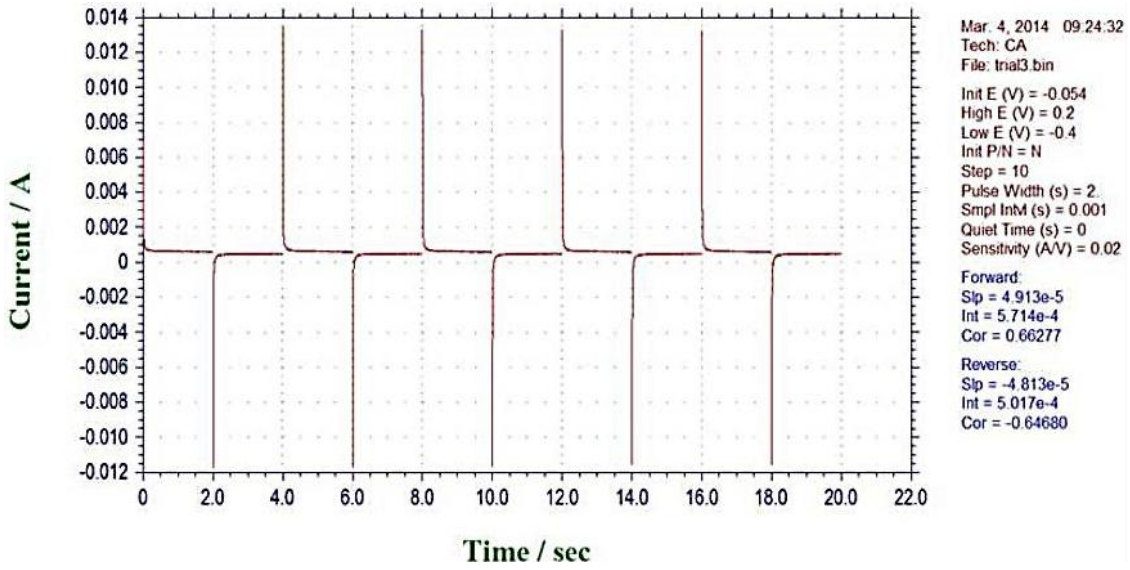

Figure 2.14 Chronoamperometry plot of the applied potential steps.

2.4.2 Optical detection of DNA dynamics

An ultrasensitive wide field fluorescence microscope (Nikon Eclipse TiE) (as shown in Figure 2.15) described previously[13] was employed for optical detection of the DNA dynamics. Carbon electrodes, which were modified with 35 base-pair ds-DNA, were placed in the specially designed electrochemical cell and subsequently placed on the fluorescence microscope. The FAM6 flurophore attached to the DNA strand was excited by laser light with a wavelength of 488 nm, which was directed through the optical port between the counter and reference electrodes (see Figure 1.12). The incident laser power was maintained at 500 µW in all experiments. The power was measured just prior to the epi-illumination port of the microscope. Upon entering the microscope, the laser light first reflected from a dichroic beam-splitter and then was focused into the back aperture of a 50X, 0.55 NA air objective (Nikon), which produced a broad illuminated area on the sample. Fluorescence emitted by the sample was collected with the same objective, passed back through the dichroic beam-splitter, a bandpass filter (Chroma HQ535/50M) and a 515 nm longpass filter (CVI). The fluorescence signal was then imaged onto a thermoelectrically cooled electron multiplying CCD camera (Andor, iXon DU897) and recorded as the working electrode potential was switched. Fluorescence images were recorded using conventional gain (5.1x) at a frame rate of 8 frames/s with 16x16 camera pixel binning. These conditions were selected in order to achieve a suitable signal to noise ratio.

Figure 2.15 Widefield optical microscope employed in ds-DNA reorientation studies.

Chapter 3 Concentration dependent reorientation dynamics of ds-DNA on glassy carbon electrode surfaces

3.1 Introduction

It has been illustrated that ds-DNA reorientation on electrode surfaces can be electrically induced.[13,14] By using distance-dependent quenching of a fluorescent dye attached to the distal end of the DNA strand, the orientation of DNA strands tethered onto electrode surfaces has been investigated. It has been observed that when the electropotential was switched between negative and positive potentials with respect to the OCP, the DNA strands are either repelled from the electrode surface or attracted towards the electrode surface, respectively. When the strands are repelled from the electrode surface, they reorient to an "upright" position, emitting bright fluorescence from the attached dye. As the strands are attracted towards the electrode surface, they lie parallel to the surface and hence, strong quenching of the fluorescence occurs (see Figure 3.1).

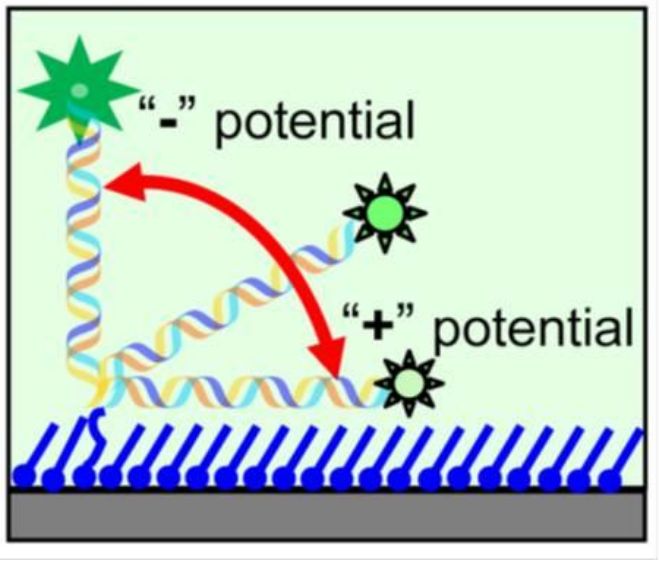

Figure 3.1 ds-DNA orientation. Reprinted with permission from ref 13. Copyright 2012 American Chemical Society.

Much of the previous work investigating potential dependent reorientation of electrode bound DNA suggests that the reorientation process and observed changes in fluorescence signal

occur very rapidly, and that the fluorescence intensity remains constant after a potential step. More recently, the Li and Higgins groups have demonstrated that a slow decay in the fluorescence occurs after each potential step.[13] Figure 3.2 provides representative data. We observed similar fluorescence modulation with an applied electric field but noted faster decay of the fluorescence signal with positive applied bias and slower switching of the signal with negative applied bias in contrast to that observed by Q. Li, et al.[13] Figure 3.3 provides representative data.

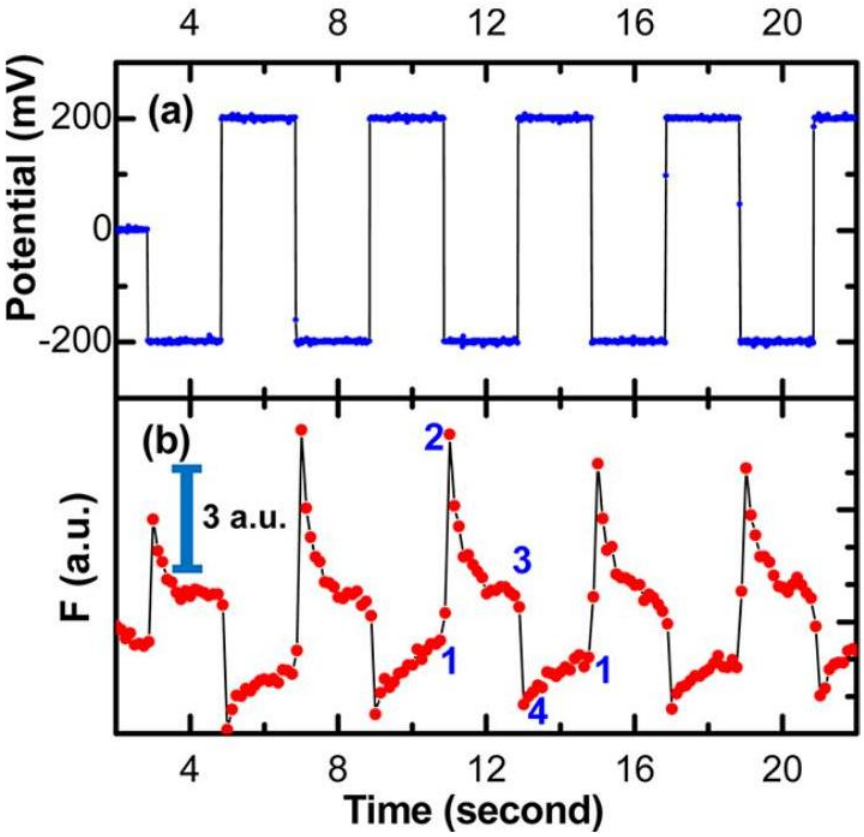

Figure 3.2 Representative potential waveform applied to the GCE and background corrected fluorescence intensity profile obtained from FAM6-labeled 34-mer ds-DNA attached to GCE in 0.02X PBS. Reprinted with permission from ref 13. Copyright 2012 American Chemical Society.

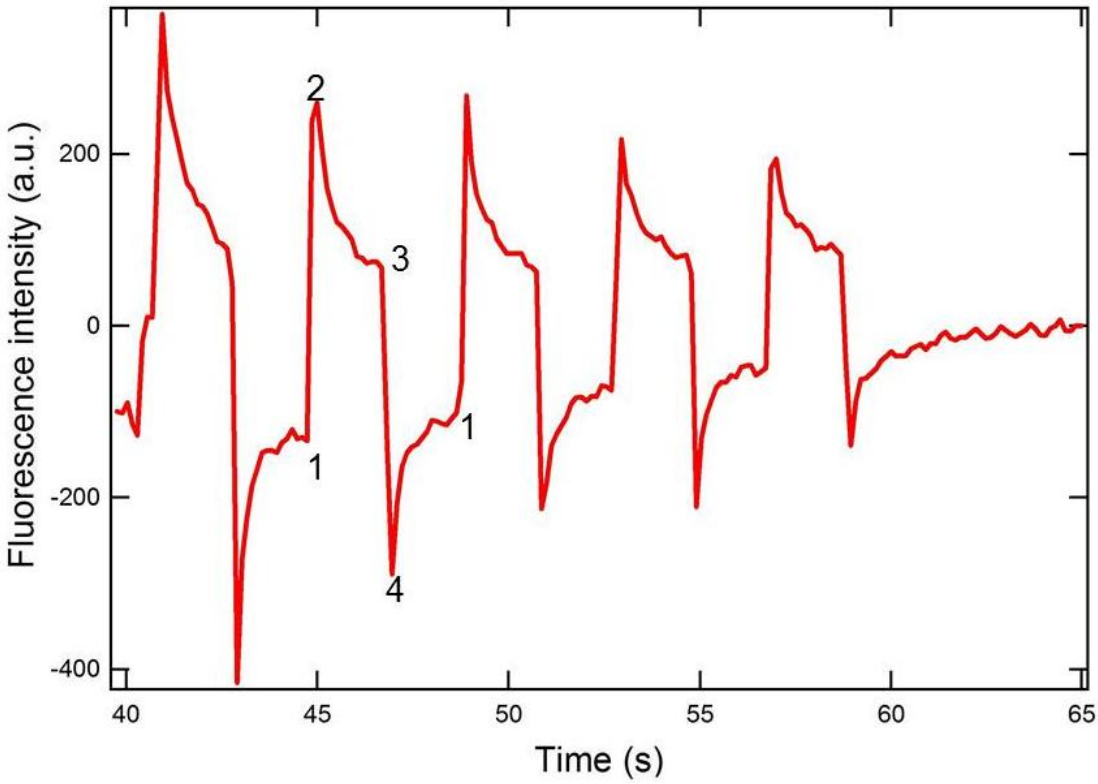

Figure 3.3 Background corrected fluorescence intensity profile obtained from a FAM6 labeled 35-mer ds-DNA attached to GCE.

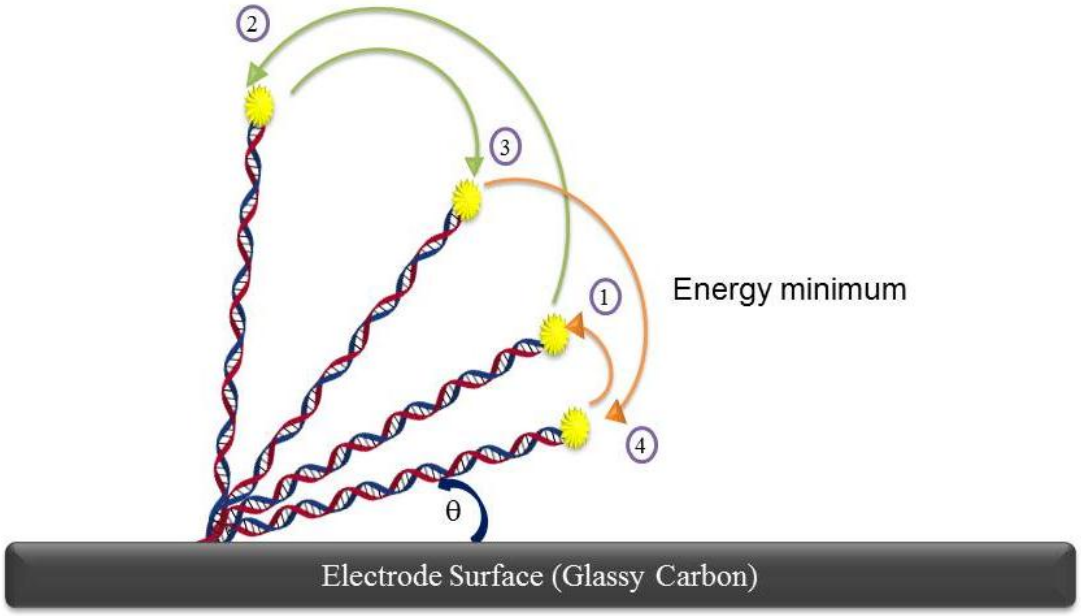

Figure 3.4 Model of DNA switching and reorientation with the applied potential steps.

Figure 3.4 illustrates the orientations of the ds-DNA molecules that qualitatively describe the ds-DNA orientation state on the fluorescence profile shown in Figure 3.3. Initially, the ds-DNA attached to the electrode surface would statistically reside around position 1, the approximate minimum energy position for positive electrode potentials. This position is determined by the equilibrium between the Brownian motion of the DNA and the electrostatic interactions. It represents a relaxed orientation state at which the ds-DNA molecules remain tilted to some extent from the surface of the electrode. Because of close proximity between the dye label and the electrode, the observed fluorescence is low. When a negative potential is applied, the DNA rapidly reorients to an upright position, designated position 2. The ds-DNA is presumed to be oriented vertical to the electrode surface at this point. The dye label is now at its maximum distance from the GCE electrode, giving minimum quenching and maximum fluorescence. The ds-DNA next relaxes towards position 3. The origins of this relaxation are unknown at present. When a positive potential is applied, the DNA strands are again attracted towards the electrode surface and quickly reorient from 3 to 4. In the latter, they initially align parallel to the electrode surface. As the fluorescent dye moves near to the electrode surface, the fluorescence signal drops to its minimum value. Once again, the DNA strands subsequently appear to relax towards position 1. When the ds-DNA strand relaxes, the fluorescence signal observed increases gradually. The origins of this relaxation are also unknown at present. The tilt angle (θ, which is related to the dye-metal distance normal to the surface plane) (see Figure 3.4) associated with position 3 is much greater than that at position 1 due to the fact that at position 3, the strands are subjected to repulsive forces. At position 1, the strands encounter attractive electrostatic forces, where both forces are in equilibrium with thermal ds-DNA motions.

The Higgins and Li groups have developed several hypotheses to explain the origins of the slow relaxation from positions $2 \rightarrow 3$ and $4 \rightarrow 1$. First, it is possible they arise from artifacts. Namely, it is well known that FAM6 fluorescence is pH sensitive and that the pH near the electrode surface may change dramatically with potential, especially for relatively dilute PBS buffers. Second, it may result from steric crowding of the DNA on the surface. Third it may be due to DNA homology in which electrostatic attractions arise between the ds-DNA molecules. In this chapter, we seek to explore these hypotheses further. The former is examined by changing the buffer and cell geometry, the latter two by varying the surface concentration of DNA.

3.2 Results

3.2.1 General observations

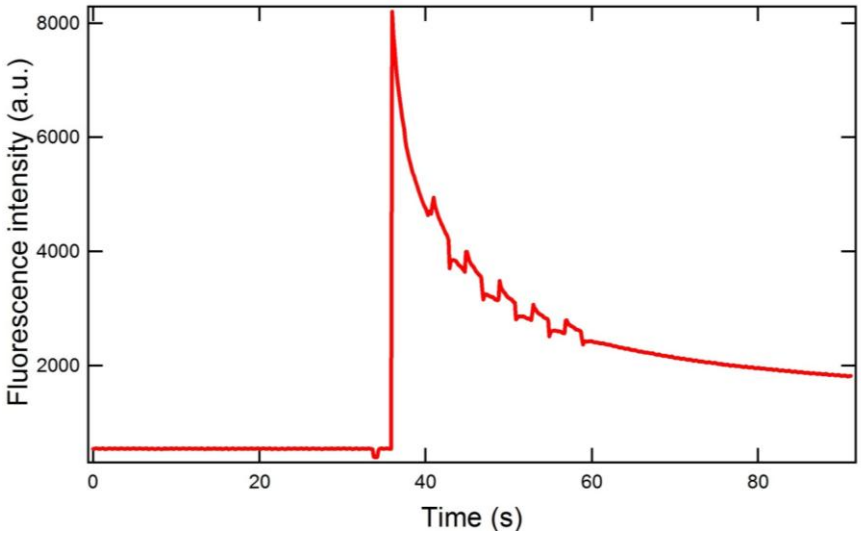

Figure 3.5 Raw data before eliminating the background.

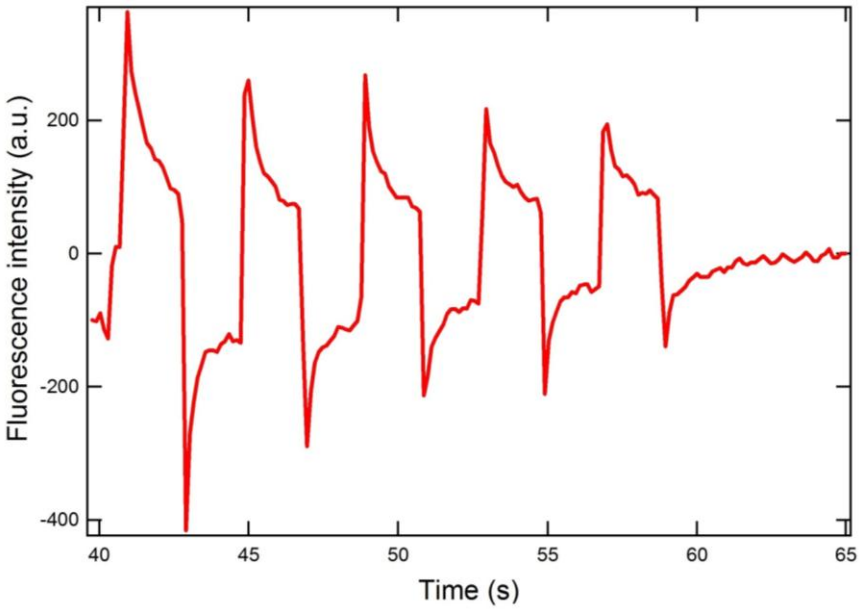

Figure 3.6 The corrected signal after eliminating the background mathematically.

As mentioned previously, the GCE was modified with 35 base-pair ds-DNA, where the 3' end was linked to the electrode surface, while the 5' end was labeled with the FAM6 fluorophore. The fluorophore was excited by laser light of wavelength of 488 nm and the photon emission was detected with the use of a thermoelectrically cooled CCD camera. The potential step was first applied after the CCD camera had stabilized. Therefore, the CCD camera was turned on first. Then, after a few frames have elapsed (~275), the laser shutter was opened. This lead to a rapid increase in the fluorescence signal. Figure 3.5 shows the raw fluorescence profile obtained from FAM6-labeled 35-mer ds-DNA in 3 mM potassium phosphate buffer. This plot depicts a relatively large exponentially decaying background that is also observed in the absence of dye labeled DNA. While its origins are uncertain, it is attributed to bleaching of both the FAM6 label and impurities adsorbed on the electrode surface.

The corrected fluorescence signal after the background has been removed is presented in Figure 3.6. The decay can be eliminated mathematically or experimentally. When eliminating the background mathematically, we fit the background to an exponential function by using a program written in the Igor Program environment. Once the decay was removed, we see that the fluorescence increased when the potential was stepped to -0.4 V and dropped upon switching to +0.2 V. The fluorescence signal did not remain at a constant level during the potential switching. Thus, even with the use of new cell geometry and better buffer, the dynamics observed were qualitatively similar to the dynamics observed by Q. Li, et al.[13] This indicates that cell geometry issues and pH effects are not the dominant cause of the previously observed dynamics. The slight differences observed on the positive side may be due to counter electrode effects (see appendix), or they may arise from a reduction in pH artifacts due to the better buffer.

3.2.2 Buffer capacity and changes in signal

As shown by Q. Li, et al.,[13] pH artifacts are expected to be greatest at positive potentials, where acid is generated at the GCE. Here, the PBS buffer used by Qin Li was replaced with a phosphate buffer (3 mM phosphate buffer which is comprised of 0.672 mM KH_2PO_4 and 2.33 mM K_2HPO_4) of greater buffer capacity.

Buffer capacity is a quantitative measure as to how well a solution will resist a change in pH with the addition of a strong acid or base. Buffer capacity (β) is defined by:

$$\beta = \frac{-dC_a}{dpH} = \frac{dC_b}{dpH}$$

where C_a and C_b are the number of moles of strong acid and base per liter needed to produce a unit change in the pH of the solution. If the value of β is large, the solution will be more resistant to pH changes. The buffer capacity for 0.02X PBS (ionic strength 3.315 mM) was determined to be $7.1x10^{-5}$ moles H^+/L x pH while that of 3 mM phosphate buffer (ionic strength 7.662 mM) was found to be $1.0x10^{-3}$ moles H^+/L x pH. Thus, the buffer capacitance of the phosphate buffer was found to be 14x higher than 0.02X PBS buffer.

3.2.3 Probe concentration dependence

The dynamics observed may be due to high DNA coverage on the electrode surface and associated steric interactions. To investigate this hypothesis, the dynamics of 35-mer ds-DNA reorientation were studied for samples prepared using three different probe concentrations: 0.25, 1.0 and 1.5 μM. These represent the concentrations employed during electrode functionalization.

3.2.3.1 Surface density of DNA on glassy carbon electrode surface

An electrochemical method has been developed by Steel and co-workers to quantify the density of DNA immobilized on gold electrode surfaces.[41] The density of both single and double stranded DNA on electrode surfaces can be determined by this method. The same method was applied here to determine DNA density on GCE surfaces. For this purpose, DNA modified electrodes were exposed to 50 μM hexammineruthenium(III) chloride in 10 mM Tris-HCl buffer (pH 7.4). The $Ru(NH_3)_6^{3+}$ binds to the phosphate backbone of the DNA under these conditions. Each $Ru(NH_3)_6^{3+}$ binds to three phosphate groups on the DNA and all of the negative charge associated with the DNA is assumed to be neutralized. By using chronocoulometry, the amount of the charge needed to reduce the redox marker in the DNA layer can be determined. The measured charge is directly proportional to the concentration of phosphate groups and thus the surface density of the DNA.

Considering a planar electrode with adsorbed redox markers, the total charge (Q) measured using chronocoulometry represents the sum of that required for double layer charging (Q_{dl}), electrolysis of freely diffusing redox markers in solution ($Q_{diffuse}$) and the electrolysis of the redox markers adsorbed to the surface (Q_{ads}). A change in the potential is always accompanied by rearrangement of the ions in the double layer. This leads to a contribution to the signal from capacitive current (Q_{dl}). The fact that only a short time is required after the potential step to charge the double layer, allows for the double layer charge, Q_{dl} to be distinguished from the

charge due to diffusion, $Q_{diffuse}$. Diffusion of free species in solution is relatively slow and occurs on a much longer time scale. For the diffusing redox component, the current response is given by the Cottrell equation:

$$i = \frac{n\ F\ A\ C_0\ D_0^{1/2}}{\pi^{1/2} t^{1/2}}$$

The charge Q can be obtained by integrating the current *i* as a function of time *t* and is given by the integrated form of the Cottrell equation:

$$Q_{diffuse} = \frac{2\ n\ F\ A\ C_0\ D_0^{1/2}\ t^{1/2}}{\pi^{1/2}}$$

The charge associated with the surface adsorbed redox component is given by:

$$Q_{ads} = n\ F\ A\ \Gamma_0$$

While the total charge is:

$$Q_{total} = Q_{ads} + Q_{dl} + Q_{diffuse}$$

The chronocoulometry plot, also known as an Anson plot,[42] depicts Q_{total} vs $t^{1/2}$. A representative example is given in Figure 3.7. The intercept at $t^{1/2} = 0$ is the sum of the double layer charging and the term related with the surface excess of bound Ru^{3+}. By obtaining the difference in the chronocoulometric intercepts in the presence and absence of the redox marker, the surface excess of the redox marker, Γ_0, can be determined. Γ_0 has units of moles/cm^2.

The complete charge compensation of DNA can be converted to the amount of DNA surface density through the following relationship:

$$\Gamma = \frac{\Gamma_0\ z\ N_A}{m} = \left(\frac{Q_{ads}}{n\ F\ A}\right) * \left(\frac{z}{m}\right) *\ N_A$$

where Γ is the surface density in DNA molecules/cm^2, n is the number of electrons associated with the redox reaction per molecule (1), z is the charge of the redox molecule (3), m is the total number of bases in the oligonucleotide (35 for ss-DNA and 70 for ds-DNA), and N_A is Avogadro's number..

Electrodes modified with both 35-mer ss-DNA and ds-DNA with varying probe concentrations of 0.25 μM, 1.0 μM and 1.5 μM were investigated using the same electrochemical Teflon cell. Figure 3.7 and Figure 3.8 show chronocoulometry plots obtained for 35-mer ss-DNA and ds-DNA, respectively, with a probe concentration of 1.0 μM. The Q_{ads} for ss-DNA is 0.4678 μC and for ds-DNA it is 0.7341 μC. This corresponds to a ss-DNA density of 3.525×10^{12} cm^{-2}. The average spacing between DNA molecules is 5.3 nm in this case. For ds-DNA, a density of 2.766×10^{12} cm^{-2} was obtained, yielding an average spacing of 6.0 nm. Table 3.1 provides a summary of the results obtained for the three different probe concentrations. The average ds-DNA reported by Q. Li, et al. was 1.8×10^{12} cm^{-2} with an average spacing of 8.0 nm.[13] The data shown in Table 3.1 demonstrate that the surface coverage increases with increasing probe concentration, as expected following a Langmuir isotherm.[43] The differences in the ss- and ds-DNA surface coverages may be due to the fact that functionalization and hybridization efficiencies differ considerably due to geometric factors of the probe and the probe/target duplex. A summary on the variations in the OCP for 35-mer ds-DNA modified GCE as a function of the probe concentration and ds-DNA density is shown in
Table 3.2.

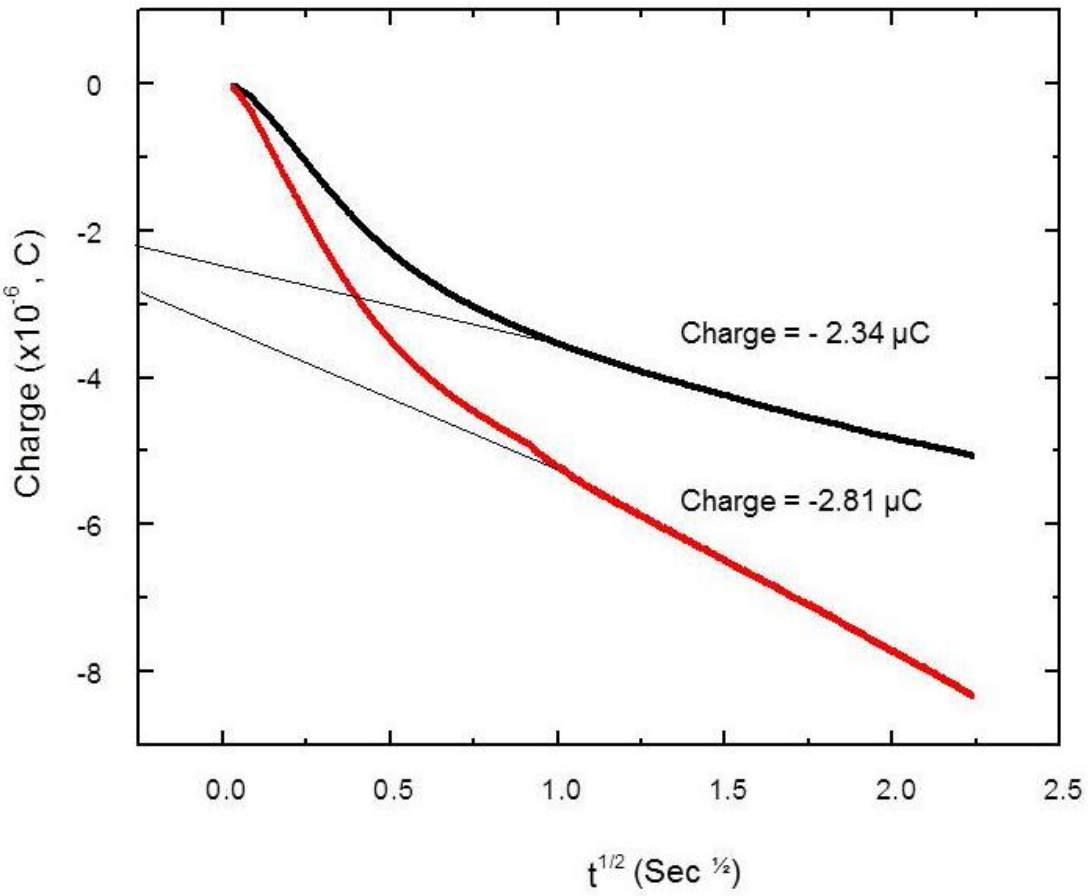

Figure 3.7 Chronocoulometry plot for determining the density of ss-DNA of 35-mer with a probe concentration of 1.0 µM. The black line is the measurement without Ru(III) and the red line with Ru(III).

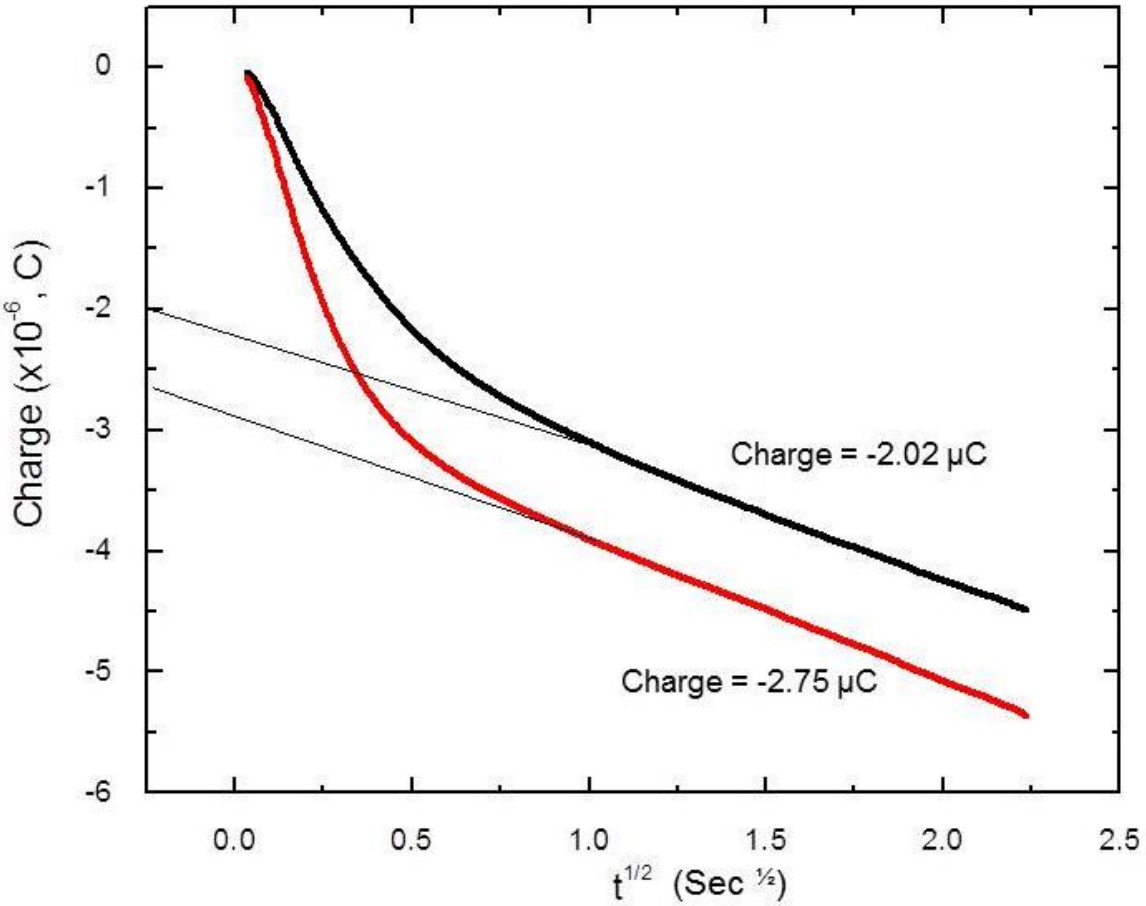

Figure 3.8 Chronocoulometry plot for determining the density of ds-DNA of 35-mer with a probe concentration of 1.0 µM. The black line is the measurement without Ru(III) and the red line with Ru(III).

Probe concentration	**ss-DNA density (ss-DNA/cm^2)**	**Average ss-DNA density (ss-DNA/cm^2)**	**ds-DNA density (ds-DNA/cm^2)**	**Average ds-DNA density (ds-DNA/cm^2)**
0.25 µM				
Set 1	$3.5x10^{12}$	**$3.34x10^{12}$**	$1.8x10^{12}$	**$1.18x10^{12}$**
Set 2	$3.2x10^{12}$		$5.6x10^{11}$	
1.0 µM				
Set 1	$3.5x10^{12}$	**$3.61x10^{12}$**	$2.8x10^{12}$	**$3.25x10^{12}$**
Set 2	$3.7x10^{12}$		$3.7x10^{12}$	
1.5 µM				
Set 1	$4.5x10^{12}$	**$4.67x10^{12}$**	$5.0x10^{12}$	**$4.26x10^{12}$**
Set 2	$4.8x10^{12}$		$3.5x10^{12}$	

Table 3.1 Summary of calculated DNA densities of ss-DNA and ds-DNA for the different probe concentrations.

Concentration of probe (µM)	ds-DNA density (cm^{-2})	Measured OCP vs. Ag/AgCl quasireference electrode (V)
0.25	$1.18x10^{12}$	0.0383± 0.0257
1.0	$3.25x10^{12}$	0.0076± 0.0051
1.5	$4.26x10^{12}$	-0.0143± 0.0058

Table 3.2 Variations in the OCP for 35-mer ds-DNA modified GCE as a function of probe concentration and ds-DNA density.

3.2.3.2 Concentration dependence of DNA reorientation

Figure 3.9 shows the background-corrected fluorescence profiles obtained from FAM6 labeled 35-mer ds-DNA at the three different probe concentrations. We observed the same trend in the fluorescence signal as observed in previous studies.[13,14] The fluorescence signal increased when the potential was stepped to -0.4 V and dropped upon switching to +0.2 V. Nevertheless, the fluorescence signal obtained did not remain at constant levels after potential switching. The same trend in the fluorescence signal was observed in all three concentrations of the probe.

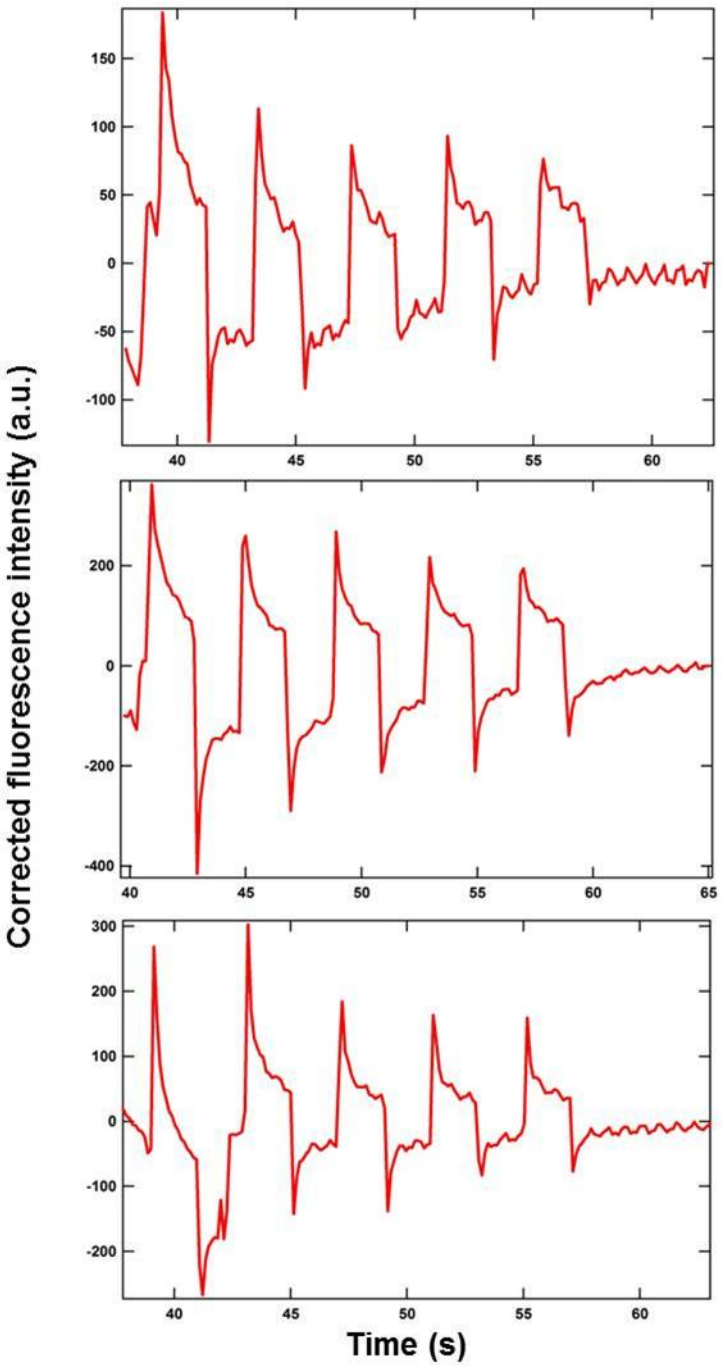

Figure 3.9 The fluorescence modulation of 35-mer ds-DNA at the three different probe concentrations. From top to bottom concentrations are 0.25, 1.0 and 1.5 µM.

3.2.3.3 Reorientation time constant of DNA reorientation dynamics

The fluorescence decays following a change in potential were fit to an empirically selected exponential decay to determine the characteristic time scale for signal relaxation. The exact expression employed was:

$$F = F_0 + A^* \exp\left(\frac{t_0 - t}{\tau}\right)$$

where the decay time constant τ is related to the reorientation time of the DNA. A faster reorientation is designated by a smaller value of τ.

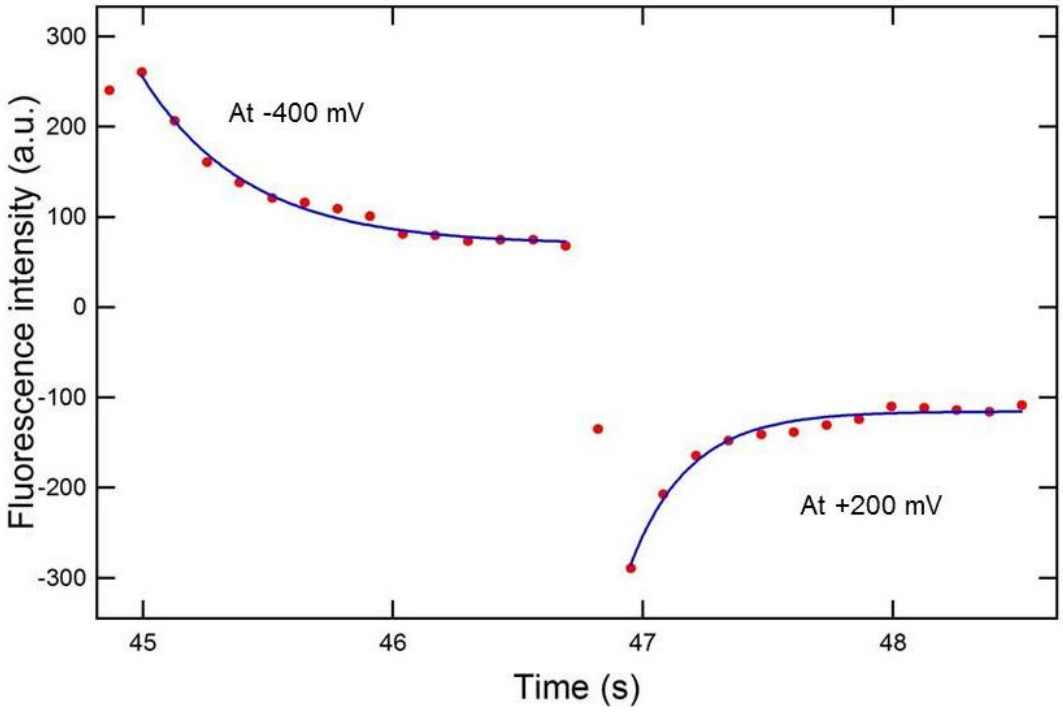

Figure 3.10 Fluorescence profile obtained during electrical switching of 35-mer ds-DNA on a GCE in 1.0 µM probe concentration. The profile has been fitted to an exponential function.

Figure 3.10 shows a representative fluorescence profile for 35-mer ds-DNA obtained for a probe concentration of 1.0 µM in 3 mM phosphate buffer solution. The points depict the data, the solid lines their fits. In each fit, the starting point was fixed to the time the potential bias was switched. The fitted values of the decay amplitude as well as the offset can potentially be used in the analysis of the FAM6 fluorescence.[13] Here, only the time scale for signal relaxation was

employed. The relaxation time following a potential step to -0.4 V was 0.41 s in the data shown. That following a step to +0.2 V was 0.25 s. It is evident that the relaxation time following a potential step to +0.2 V was shorter than the relaxation time following a potential step to -0.4 V. This general trend is borne out through a large number of replicate measurements on several different samples.

These experiments were repeated for 3 samples on 3 days for the 3 different DNA functionalization concentrations (0.25, 1.0 and 1.5 μM). Figure 3.11 and Figure 3.12 show summaries of the reorientation times at positive and negative applied potential steps, and Figure 3.13 and Figure 3.14 shows summaries of the reorientation time variation with ds-DNA density at applied positive and negative potential steps, respectively for 35-mer ds-DNA. These plots illustrate that the decay constants vary with probe concentration. They also indicate the dissimilar manner in which the decay constants vary for applied positive and negative biases. Specifically, the relaxation time constant under applied positive bias became larger as the probe concentration was increased from 0.25 μM to 1.5 μM of 35-mer DNA, implying a slowing of the dynamics. In contrast, the relaxation time constant revealed an opposite trend upon switching to negative bias. That is, the relaxation time became shorter as the probe concentration was increased.

The slopes of the plots shown in Figure 3.11and Figure 3.12 differ from zero at 90% and 99.99% confidence levels respectively. Thus, there is 90% and 99.99% certainty that the trends shown are real. While the origins of this difference are unknown it is possibly due to the electrostatic attractions between ds-DNA and steric interactions which arise between DNA strands.

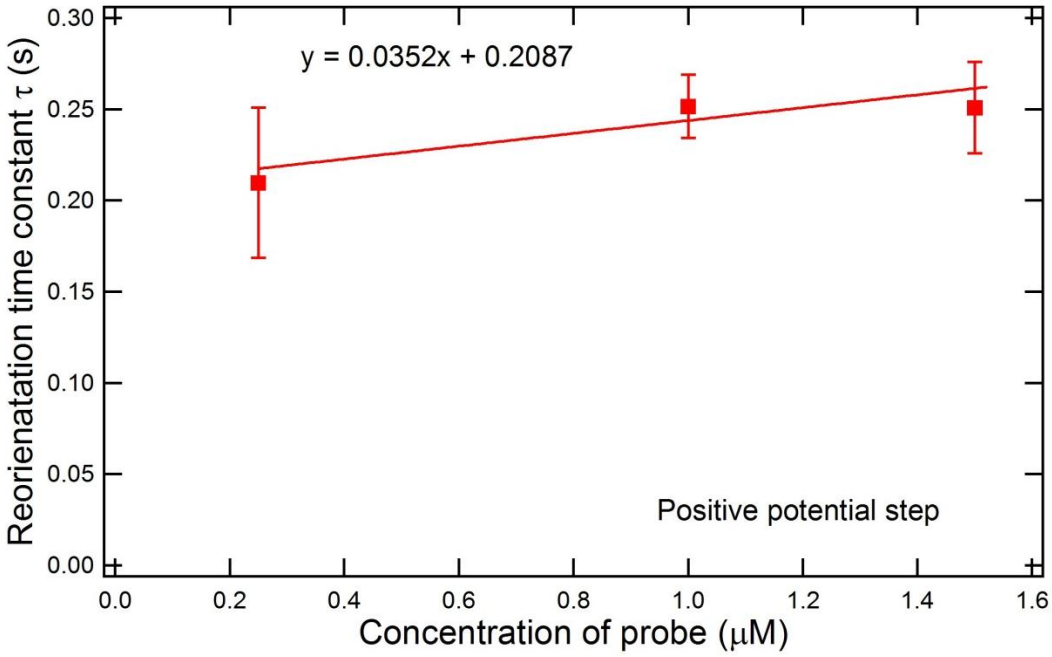

Figure 3.11 The reorientation time constant vs. concentration of probe at positive potential steps for 35-mer ds-DNA.

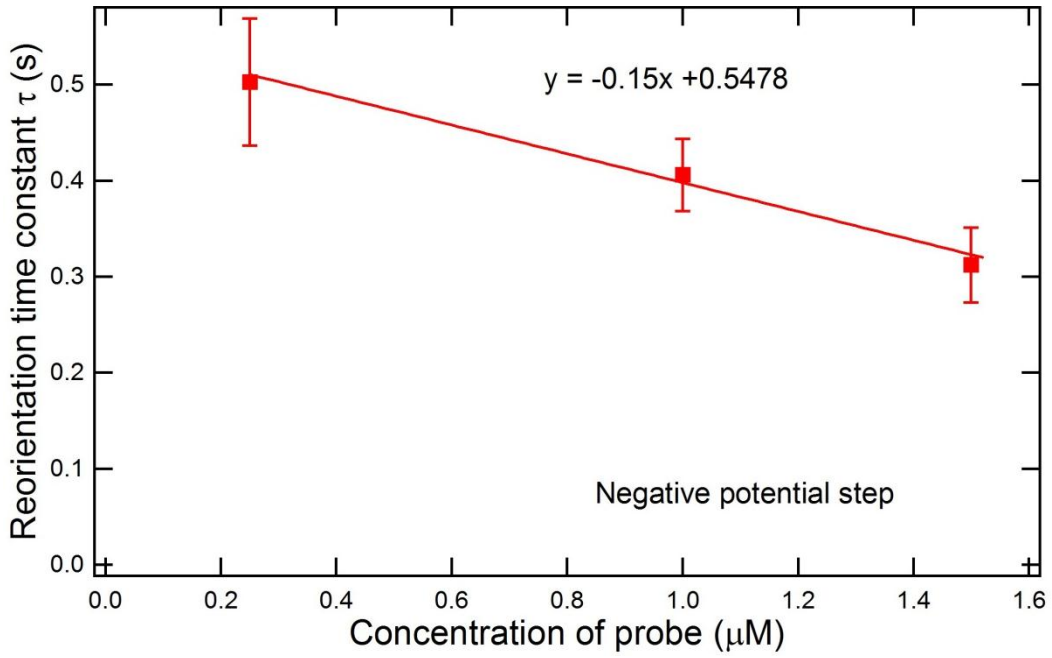

Figure 3.12 The reorientation time constant vs. concentration of probe at negative potential steps for 35-mer ds-DNA.

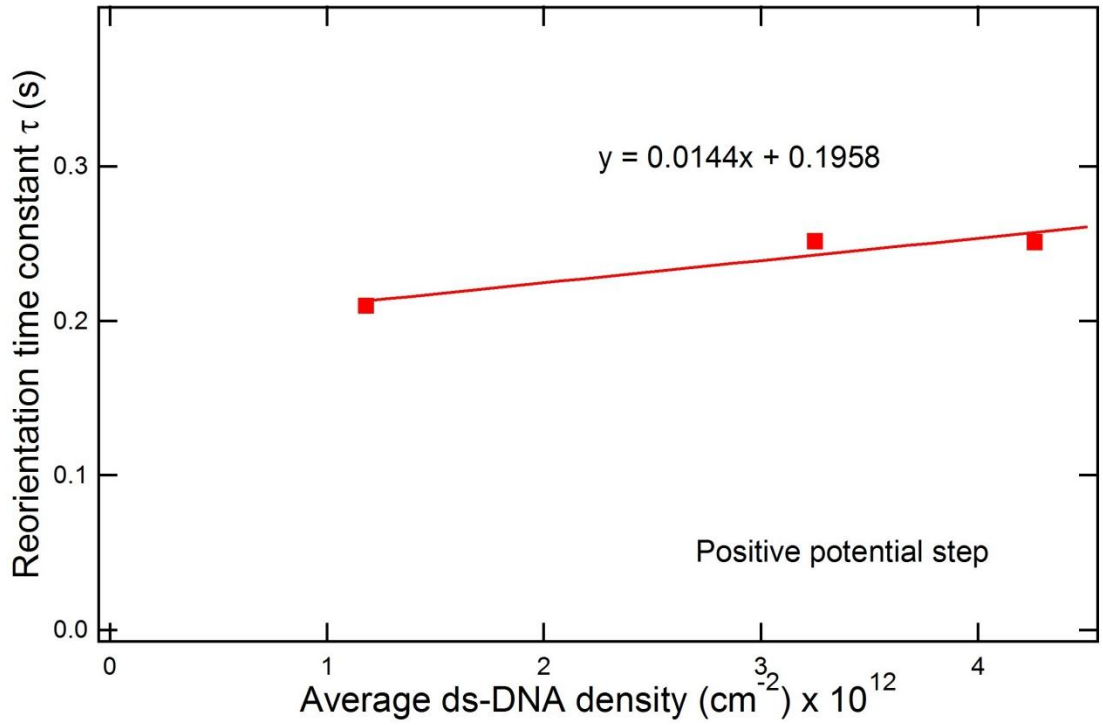

Figure 3.13 The reorientation time constant vs. average ds-DNA density at positive potential steps for 35-mer ds-DNA.

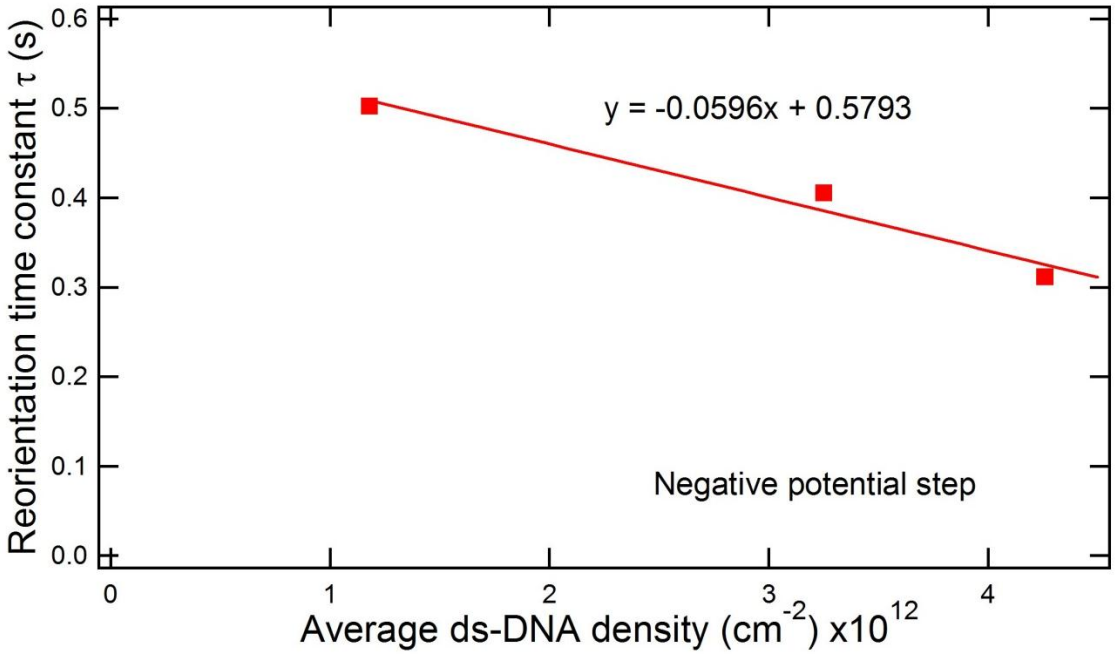

Figure 3.14 The reorientation time constant vs. average ds-DNA density at negative potential steps for 35-mer ds-DNA.

3.3 Discussion

A summary of the general observations observed in the DNA switching experiment is given in Table 3.3.

1	The orientation of DNA strands tethered on to GCE surfaces are governed by the applied electric field.
2	Probe concentration is an important parameter in the reorientation dynamics of DNA tethered to electrode surfaces.
3	The reorientation time constant increases with the increasing concentration of the probe with positive applied bias.
4	The reorientation time constant decreases with the increasing concentration of the probe with negative applied bias.
5	In comparison with previous work, we observed fast switching of the fluorescence signal with applied positive potential with a smaller time constant and slower decay of the switching/signal with the applied negative potential with a larger time constant.

Table 3.3 Summary of observations.

3.3.1 Time constant of DNA reorientation dynamics

These studies were undertaken to determine how the surface concentration of DNA impacts the switching dynamics. The exact origins of the dynamics observed are unknown, but several possible explanations exist. It was previously proposed that strong steric interactions between DNA strands may be the cause of slow relaxation.[13] The observed switching dynamics may also be due to attractive forces that arise between the ds- DNA molecules as shown in Figure 3.15.

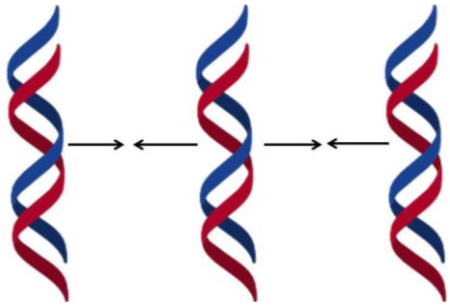

Figure 3.15 Attractive forces between DNA strands.

The simplest form of the assembly of nucleic acids is considered to be the double helix when a single stranded DNA pairs with a strand consisting of its complementary nucleotide sequence. However, it has been reported in the literature that DNA strands can also form triplex and quadruplex structures through base pairing.[44] Many studies have also shown that other attractive forces also exist between ds-DNA molecules.[45,46,47,48,49,50] Previous studies have demonstrated that the presence of oppositely charged ions associated with the DNA also lead to attractive interactions between neighboring DNA strands. These interactions occur between the anionic phosphate groups and their associated counter ions. However, polyvalent counterions are usually required for such DNA attractions.[48,49] Recent studies have shown that attraction homology can occur through electrostatic interactions between homologous DNA sequences, even in the absence of polyvalent counterions.[49] DNA attraction can occur due to correlations in the charge distributions between neighboring ds-DNA molecules. According to this theory, the charge distributions include the phosphate in the DNA as well as the monovalent and/or any divalent ions bound to/or in close proximity to the DNA molecules.

The interactions between the highly charged DNA molecules are mainly electrostatic as shown in Figure 3.16. These DNA-DNA interactions depend on charge density as well as the double helix structure. Efficient pairing will occur between fairly short homologous regions.

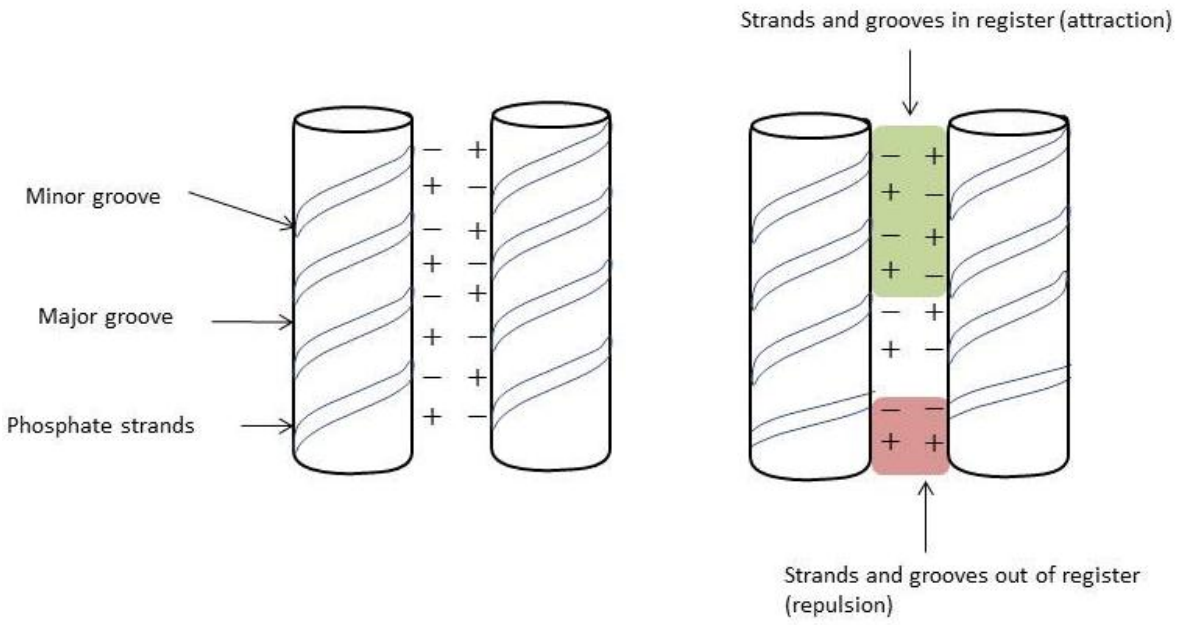

Figure 3.16 Model for the DNA-DNA attractions. Modified from ref 51.

The model shown in Figure 3.16 illustrates the manner in which two homologous DNA strands recognize each other electrostatically. The electrostatic attraction occurs between the negatively charged strands facing the positively charged grooves arise from the condensation of counter ions in these regions. According to Kornyshev, et al.,[51] a DNA strand with 35 base-pairs should exhibit close to $0.5k_BT$ interaction energy. It has been reported in the literature that the strength of electrostatic interactions has an impact in determining the orientation of ds-DNA.[52]

The mobility of ds-DNA initiated by an applied electric field is strongly affected by the surface coverage.[20] If the DNA strands are closely spaced, strong interactions will restrict the range of accessible strand orientation and will also limit dynamic DNA strand reorientation. It has been stated in previous work[14,22] that only ds-DNA present at low surface coverage exhibit a fast response to a change in the electropotential. These strong interactions will lead to slower reorientation dynamics.

At low surface coverage (i.e.; with 0.25 μM probe concentration with a ds-DNA density of 1.18×10^{12} cm^{-2}), the strands are separated by an average of 9.2nm distance. But with high surface coverage (i.e.; with 1.5 μM probe concentration with a ds-DNA density of 4.26×10^{12} cm^{-2}), the DNA-DNA spacing is smaller, having an average of 4.8nm. These distances are shorter than the extended length of the ds-DNA, indicating that when they orient parallel to the surface

under positive applied bias, the strands will overlap to some extent and could therefore interact by the above mechanism. At applied negative potentials, neighboring ds-DNA strands may approach each other and interact electrostatically. Hence, even under negative bias, some tilting of the ds-DNA from the surface normal is expected.

Based on the above model and considerations, we believe that attractive interactions between the ds-DNA best explain the observed concentration dependence of the dynamics. Due to the strong attractive forces which exist between the strands, with the application of a positive bias, slow dynamics is observed. With the application of a negative bias, fast switching of the dynamics is observed. Strong interactions occur between the DNA molecules and these interactions form an energy barrier that must be overcome for the ds-DNA molecules to relax away from the surface.

The homology interactions provide the best model at present for the dynamics observed at applied positive and negative bias.

Chapter 4 Conclusion and Future Work

The field-induced reorientation of fluorescently labeled, electrode-bound ds-DNA on GCE surfaces has been studied in this thesis. Switching the electropotential between positive and negative potentials with respect to the OCP, lead to the modulation of the fluorescence from the dye label, which is due to distance dependent quenching to the electrode surface. We observed the same fast initial switching dynamics as observed by others and also verified the slow relaxation dynamics first reported by Q. Li, et al.[13] Building upon the work of Qin Li, we explored the concentration dependence of the slow relaxation dynamics.

We designed an electrochemical cell using a platinum (Pt) coated patterned ITO coverslip and PDMS that differs significantly from that used by Qin Li. We have shown that regardless of the electrochemical cell design, the slow relaxation dynamics of double stranded DNA attached to a GCE can be observed. We also used a different buffer to minimize any pH effects on the FAM6 fluorophore.

We have shown that the reorientation time constant increases with increasing DNA probe concentration under positive applied potential (vs. OCP) indicating slower switching of the signal, while under negative applied potential (vs. OCP), the reorientation time constant decreases with increasing DNA probe concentration, indicating faster switching of the signal.

Future studies of DNA dynamics on GCEs will include investigation of the dynamics using different phosphate buffer strengths (i.e., 10 mM potassium phosphate) as well as DNA strands with a different length (i.e., 45-mer). Should the proposed mechanism properly explain the concentration dependence of the dynamics, the DNA interactions should only become stronger for longer DNA molecules. We can also investigate the similarities in the trend of the reorientation time constant with probe concentration using PBS buffer.

Future studies of DNA dynamics should also include investigations using planar gold (Au) electrodes, with comparison of the results to those from GCEs. Although such studies have already been investigated on gold electrodes, performing the experiment using the optical setup we employed will ensure that the results are comparable with previous work. It should be remembered that the slow relaxation observed by Li, et al. and verified here have not been reported previously on gold. The method of DNA attachment and the electrode material will be the only differences between the studies. Thus it could lead to new insights on the importance of

the role played by the charged DNA molecules in the EDL and in controlling/limiting their own dynamics.

Overall a much deeper understanding is still required on the roles played by the EDL, the steric effects and the structure of the GCE to acquire more knowledge on the field-induced dynamics of electrode-bound DNA.

References

[1] Sassolas, A.; Leca-Bouvier, B. D.; Blum, L. J. *Chem. Rev.* **2008**, *1*, 109-139.

[2] Chen, J.; Zhang, J.; Huang, L.; Lin, X.; Chen, G. *Biosensors and Bioelectronics* **2008**, *3*, 349-355.

[3] Cagnin, S.; Caraballo, M.; Guiducci, C.; Martini, P.; Ross, M.; SantaAna, M.; Danley, D.; West, T.; Lanfranchi, G. *Sensors* **2009**, *4*, 3122-3148.

[4] Komarova, E.; Aldissi, M.; Bogomolova, A. *Biosensors and Bioelectronics* **2005**, *1*, 182-189.

[5] Pividori, M.; Merkoci, A.; Alegret, S. *Biosensors and Bioelectronics* **2000**, *5*, 291-303.

[6] Tornow, M.; Arinaga, K.; Rant, U. *NanoBioTechnology* **2008**, pp 187-214.

[7] Kuhr, W. G. *Nat. Biotechnol*, **2000**, *10*, 1042-1043.

[8] Gebala, M.; Schuhmann, W. *Physical Chemistry Chemical Physics* **2012**, *43*, 14933-14942.

[9] Kjällman, T. H.; Peng, H.; Soeller, C.; Travas-Sejdic, J. *Anal. Chem.* **2008**, *24*, 9460-9466.

[10] Daniels, J. S.; Pourmand, N. *Electroanalysis* **2007**, *12*, 1239-1257.

[11] Drummond, T. G.; Hill, M. G.; Barton, J. K. *Nat. Biotechnol*. **2003**, *10*, 1192-1199.

[12] Ye, Y.; Ju, H. *Sensors* **2003**, *6*, 128-145.

[13] Li, Q.; Cui, C.; Higgins, D. A.; Li, J. *J. Am. Chem. Soc*. **2012**, *35*, 14467-14475.

[14] Rant, U.; Arinaga, K.; Fujita, S.; Yokoyama, N.; Abstreiter, G.; Tornow, M. *Nano Letters* **2004**, *12*, 2441-2445.

[15] Kelley, S. O.; Barton, J. K.; Jackson, N. M.; McPherson, L. D.; Potter, A. B.; Spain, E. M.; Allen, M. J.; Hill, M. G. *Langmuir* **1998**, *24*, 6781-6784.

[16] Sosnowski, R. G.; Tu, E.; Butler, W. F.; O'Connell, J. P.; Heller, M. J. *PNAS* **1997**, *4*, 1119-1123.

[17] Heaton, R. J.; Peterson, A. W.; Georgiadis, R. M. *PNAS* **2001**, *7*, 3701-3704.

[18] Wei, F.; Qu, P.; Zhai, L.; Chen, C.; Wang, H.; Zhao, X. S. *Langmuir* **2006**, *14*, 6280-6285.

[19] Rant, U.; Arinaga, K.; Tornow, M.; Kim, Y. W.; Netz, R. R.; Fujita, S.; Yokoyama, N.; Abstreiter, G. *Biophys. J.* **2006**, *10*, 3666-3671.

[20] Rant, U.; Arinaga, K.; Fujita, S.; Yokoyama, N.; Abstreiter, G.; Tornow, M. *Langmuir* **2004**, *23*, 10086-10092.

[21] Rant, U.; Arinaga, K.; Fujiwara, T.; Fujita, S.; Tornow, M.; Yokoyama, N.; Abstreiter, G. *Biophys. J.* **2003**, *6*, 3858-3864.

[22] Rant, U.; Arinaga, K.; Scherer, S.; Pringsheim, E.; Fujita, S.; Yokoyama, N.; Tornow, M.; Abstreiter, G. *PNAS* **2007**, *44*, 17364-17369.

[23] Kaiser, W.; Rant, U. *J. Am. Chem. Soc.* **2010**, *23*, 7935-7945.

[24] Jennings, T.; Singh, M.; Strouse, G. *J. Am. Chem. Soc.* **2006**, *16*, 5462-5467.

[25] Murphy, J. N.; Cheng, A. K.; Yu, H.; Bizzotto, D. *J. Am. Chem. Soc.* **2009**, *11*, 4042-4050.

[26] Widrig, C. A.; Chung, C.; Porter, M. D. *Journal of Electroanalytical Chemistry and Interfacial Electrochemistry* **1991**, *1*, 335-359.

[27] Li, J.; Ng, H. T.; Cassell, A.; Fan, W.; Chen, H.; Ye, Q.; Koehne, J.; Han, J.; Meyyappan, M. *Nano Letters* **2003**, *5*, 597-602.

[28] Franzen, S. *Chemical Physics Letters* **2003**, *3*, 315-321.

[29] Pocard, N. L.; Alsmeyer, D. C.; McCreery, R. L.; Neenan, T. X.; Callstrom, M. R. J.*Mater.Chem*. **1992**, *8*, 771-784.

[30] Van der Linden, W.; Dieker, J. W. *Anal. Chim. Acta* **1980**, *1*, 1-24.

[31] Harris, P. J. *Critical Reviews in Solid State and Materials Sciences* **2005**, *4*, 235-253.

[32] McCreery, R. L. *Chem. Rev.* **2008**, *7*, 2646-2687.

[33] http://www.uic.edu/classes/phys/phys461/phys450/ANJUM04.

[34] Chi, Q.; Wang, G.; Jiang, J. *Physica A: Statistical Mechanics and its Applications* **2013**, *5*, 1072-1079.

[35] Geggier, S.; Kotlyar, A.; Vologodskii, A. *Nucleic Acids Res.* **2011**, *4*, 1419-1426.

[36] Taylor, W. H.; Hagerman, P. J. *J. Mol. Biol.* **1990**, *2*, 363-376.

[37] Smith, S. B.; Finzi, L.; Bustamante, C. *Science* **1992**, *5085*, 1122-1126.

[38] http://www.lifetechnologies.com/us/en/home/references/molecular-probes-the-handbook/introduction-to-fluorescence-techniques.html

[39] Chen, H.; Han, J.; Li, J.; Meyyappan, M. *Biomed. Microdevices* **2004**, *1*, 55-60.

[40] http://calctool.org/CALC/prof/bio/dna.

[41] Steel, A. B.; Herne, T. M.; Tarlov, M. J. *Anal. Chem.* **1998**, *22*, 4670-4677.

[42] http://www.asdlib.org/onlineArticles/ecourseware/Kelly_Potentiometry/PDF-7-Chronocoul.pdf

[43] Nelson, B. P.; Grimsrud, T. E.; Liles, M. R.; Goodman, R. M.; Corn, R. M. *Anal. Chem.* **2001**, *1*, 1-7.

[44] Inoue, S.; Sugiyama, S.; Travers, A. A.; Ohyama, T. *Biochemistry (N. Y.)* **2007**, *1*, 164-171.

[45] Baldwin, G. S.; Brooks, N. J.; Robson, R. E.; Wynveen, A.; Goldar, A.; Leikin, S.; Seddon, J. M.; Kornyshev, A. A. *The journal of Physical Chemistry B* **2008**, *4*, 1060-1064.

[46] Danilowicz, C.; Lee, C. H.; Kim, K.; Hatch, K.; Coljee, V. W.; Kleckner, N.; Prentiss, M. *PNAS* **2009**, *47*, 19824-19829.

[47] Cortini, R.; Kornyshev, A. A.; Lee, D. J.; Leikin, S. *Biophys. J.* **2011**, *4*, 875-884.

[48] Electrostatics, D. *Phys Today* **2000**, *9*, 38.

[49] DeRouchey, J.; Parsegian, V. A.; Rau, D. C. *Biophys. J.* **2010**, *8*, 2608-2615.

[50] Todd, B. A.; Adrian Parsegian, V.; Shirahata, A.; Thomas, T.; Rau, D. C. *Biophys. J.* **2008**, *12*, 4775-4782.

[51] Kornyshev, A.; Leikin, S. *Phys. Rev. Lett.* **2001**, *16*, 3666.

[52] Yang, X.; Wang, Q.; Wang, K.; Tan, W.; Yao, J.; Li, H. *Langmuir* **2006**, *13*, 5654-5659.

Appendix A. Additional comments

A.1 ITO as a counter electrode

Initially the experiment was performed using ITO on the patterned ITO cover glass itself as the counter electrode. We could not see the switching of the signal when a positive potential was applied (vs. OCP) as shown in Figure A. 1.

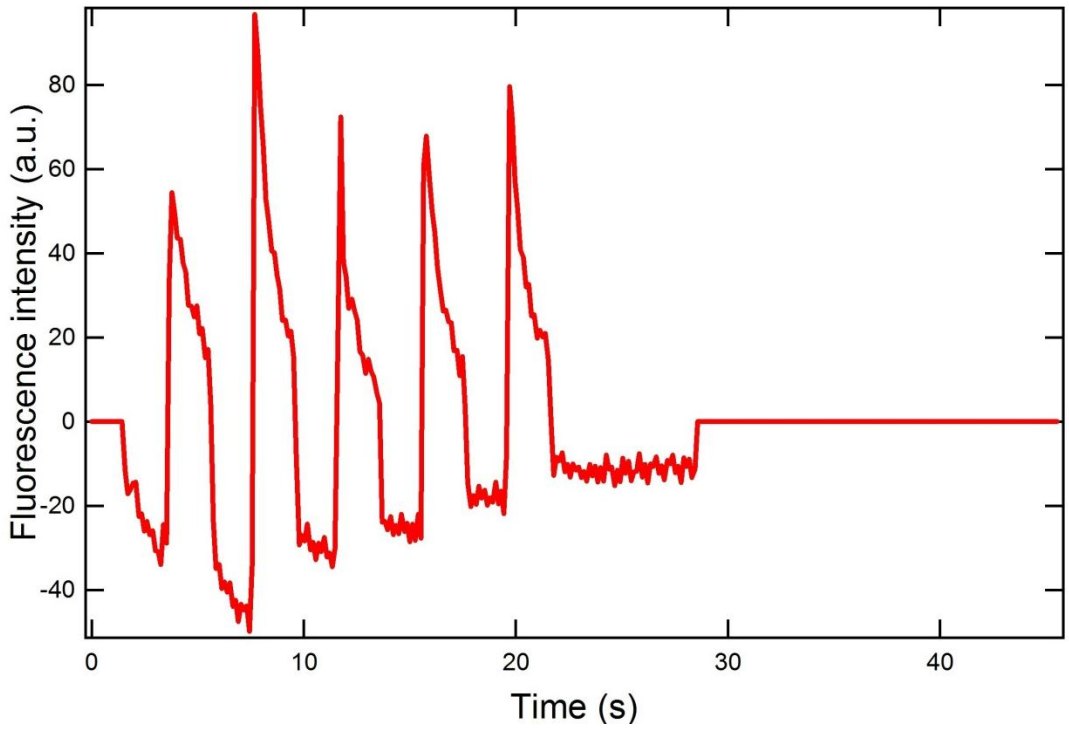

Figure A. 1 Fluorescence modulation of 35-mer ds-DNA with a probe concentration of 1.0 µM when ITO was used as the counter electrode.

Tin-doped indium oxide (ITO) is the most widely studied transparent conducting metal oxide. ITO is a heavily doped n-type semiconductor with a band gap of 3-4 eV.[53] Due to the extra electrons provided by the tin (Sn) and the oxygen vacancies, ITO has a high conductivity. The non-stoichiometric character of ITO gives an inherent heterogeneous surface to it. Thus, the defect sites play an important role on the electrical and optical properties of the ITO.

Previously, ITO films were used as electrodes in spectroelectrochemical measurements that required their conductivity as well as transparency. Recently, ITO electrodes have been used in electroanalytical sensors where the electron transfer and the surface properties of the electrode are of much importance. The surface chemistry of ITO is rather complicated due to its intrinsic

heterogeneity. It has been reported in the literature that there is a considerable change in the physical properties of ITO when exposed to an oxidative environment.[53] Oxygen vacancies are the active sites for electron transfer on ITO films. Decreasing the density of these sites will lead to slower electron transfer kinetics, a change in the electrochemical properties of the ITO. It has also been reported in the literature that ITO is unstable under high current density, which is required in fast device switching. ITO films also undergo irreversible changes followed by loss of conductivity.[53]

Bare ITO electrodes are unsuitable to be used in the optical window due to its long term stability, conductivity and transparency loss. To use ITO for stable performance we can deposit ultra-thin films of a noble metal such as Pt, Au, Ag or Pd on the ITO surface. These highly transparent layers have high electrochemical activity and stability.[54]

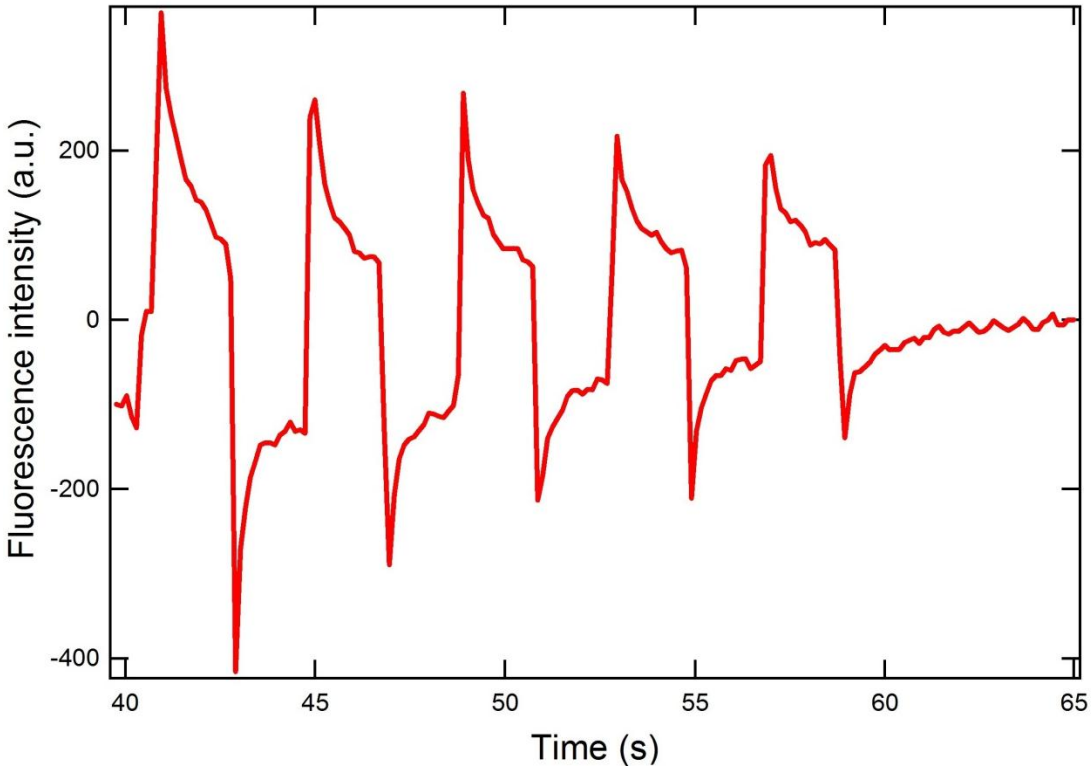

Figure A. 2 Fluorescence modulation of 35-mer ds-DNA with a probe concentration of 1.0 µM when Pt was used as the counter electrode.

As seen in Figure A. 2, when Pt was deposited on the ITO film and was used as the counter electrode, the positive side of the signal switching was observed. This shows that ITO itself may not be suitable to be used as a counter electrode in electrochemical experiments.

A.2 Facts to remember

When performing the experiment it was very clear that unless we got a good focus on the glassy carbon, we were unable to see the proper switching of the signal with the applied potentials. So we have to make sure that the laser beam is aligned and that a proper focus is obtained on the sample.

[53] Popovich, N.; Wong, S.; Ufer, S.; Sakhrani, V.; Paine, D. *J. Electrochem. Soc.* **2003**, *11*, H255-H259.

[54] Matveeva, E. *J. Electrochem. Soc.* **2005**, *9*, H138-H145.